State of the heart : the promise of pluripotent stem cell-derived cardiomyocytes in disease modelling, differentiation and development

Berg, C.W. van den

CHAPTER 3

Cardiomyocytes Derived From Pluripotent Stem Cells Recapitulate Electrophysiological Characteristics of an Overlap Syndrome of Cardiac Sodium Channel Disease

Cathelijne W. van den Berg [1,], Richard P. Davis [1,6,*], Simona Casini [1,*], Maaike Hoekstra [4], Carol Ann Remme [4], Cheryl Dambrot [1,2], Daniela Salvatori [1,3], Dorien Ward-van Oostwaard [1], Arthur A.M. Wilde [4], Connie R. Bezzina [4], Arie O. Verkerk [5], Christian Freund [1,†], Christine L. Mummery, PhD [1,6,†]*

Circulation 125: 3079-3091 (2012)

1 Department of Anatomy and Embryology, Leiden University Medical Center, Leiden, The Netherlands
2 Department of Cardiology, Leiden University Medical Center, Leiden, The Netherlands
3 Proefdiercentrum, Leiden University Medical Center, Leiden, The Netherlands
4 Department of Clinical and Experimental Cardiology, Heart Failure Research Center, Academic Medical Center, University of Amsterdam, Amsterdam, The Netherlands
5 Department of Anatomy, Embryology and Physiology, Heart Failure Research Center, Academic Medical Center, University of Amsterdam, Amsterdam, The Netherlands
6 Netherlands Proteomics Center, Utrecht, The Netherlands

*,† authors contributed equally to this article

Abstract

Pluripotent stem cells (PSCs) offer a new paradigm for modeling genetic cardiac diseases, but it is unclear whether mouse and human PSCs can truly model both gain- and loss-of-function genetic disorders affecting the Na^+ current (I_{Na}) because of the immaturity of the PSC-derived cardiomyocytes. To address this issue, we generated multiple PSC lines containing a Na^+ channel mutation causing a cardiac Na^+ channel overlap syndrome.

Induced PSC (iPSC) lines were generated from mice carrying the *Scn5a*$^{1798insD/+}$ (Scn5a-het) mutation. These mouse iPSCs, along with wild-type mouse iPSCs, were compared with the targeted mouse embryonic stem cell line used to generate the mutant mice and with the wild-type mouse embryonic stem cell line. Patch-clamp experiments showed that the Scn5a-het cardiomyocytes had a significant decrease in I_{Na} density and a larger persistent I_{Na} compared with Scn5a-wt cardiomyocytes. Action potential measurements showed a reduced upstroke velocity and longer action potential duration in Scn5a-het myocytes. These characteristics recapitulated findings from primary cardiomyocytes isolated directly from adult Scn5a-het mice. Finally, iPSCs were generated from a patient with the equivalent *SCN5A*$^{1795insD/+}$ mutation. Patch-clamp measurements on the derivative cardiomyocytes revealed changes similar to those in the mouse PSC-derived cardiomyocytes.

Here, we demonstrate that both embryonic stem cell- and iPSC-derived cardiomyocytes can recapitulate the characteristics of a combined gain- and loss-of-function Na^+ channel mutation and that the electrophysiological immaturity of PSC-derived cardiomyocytes does not preclude their use as an accurate model for cardiac Na^+ channel disease.

Introduction

Multiple cardiac arrhythmia syndromes, including long-QT syndrome type 3 (LQT3), Brugada syndrome (BrS), progressive cardiac conduction disease, and sinus node dysfunction, have been linked to mutations in *SCN5A*, the gene encoding the α-subunit of the cardiac sodium (Na^+) channel [1,2]. Most *SCN5A* mutations associated with LQT3 act by disrupting fast inactivation of the Na^+ channel, resulting in a persistent inward Na^+ current (I_{Na}) during the action potential (AP) plateau phase, subsequently delaying ventricular repolarization and prolonging the QT interval (gain-of-function mutations) [3]. In contrast, *SCN5A* mutations underlying BrS and conduction disease are loss-of-function mutations and are believed to reduce the total amount of available I_{Na} as a result of expression of nonfunctional channels, impaired intracellular trafficking, and decreased membrane surface channel expression or through altered channel gating properties [1,2].

Initially, it was believed that these arrhythmia syndromes constituted separate clinical entities, with individual *SCN5A* mutations leading to one particular electrophysiological disorder. However, genotype-phenotype studies in large pedigrees have now established that several single *SCN5A* mutations present with multiple clinical manifestations as a consequence of the various biophysical defects associated with the mutations (the so-called overlap syndromes) [4]. The first reported was the in-frame insertion of an aspartic acid residue at position 1795 in the human protein (designated 1795insD), identified in a large Dutch family, with ECG features of bradycardia, ventricular and atrial conduction slowing, LQT3, and BrS [5,6]. Transgenic mice carrying the mouse equivalent (1798insD) of the human *SCN5A*-1795insD mutation recapitulate the majority of the electrophysiological and ECG characteristics observed in patients, with $Scn5a^{1798insD/+}$ (Scn5a-het) mice displaying signs of sinus node dysfunction in addition to prolonged PQ, QRS, and QTc intervals on surface ECGs [7,8]. Patch-clamp analysis in isolated Scn5a-het cardiomyocytes demonstrated a prolonged AP duration (APD) and decreased upstroke velocity (V_{max}) compared with wild-type ($Scn5a^{+/+}$ [Scn5a-wt]) myocytes [7,8]. Additionally, the mutation resulted in a reduction in I_{Na} density, underlying the observed conduction slowing in the Scn5a-het mice. Finally, a larger persistent inward I_{Na} was measured in cardiomyocytes from Scn5a-het mice, explaining the presence of the increased APD and prolonged QTc [9]. Critically, in contrast to previous transfection studies using HEK 293 cells [10], the majority of kinetic properties of the I_{Na} remained unchanged in the isolated Scn5a-het cardiomyocytes [7,8], underscoring the challenges in interpreting the electrophysiological properties of ion channel mutations in heterologous expression systems.

The ability to reprogram somatic cells into induced pluripotent stem cells (iPSCs) and to differentiate these cells into many cell types, including functional cardiomyocytes, offers a new paradigm for modeling human disease [11,12]. However, the electrophysiological immaturity of PSC-derived cardiomyocytes (PSC-CMs) might influence whether they are able to recapitulate

Na^+ channel loss-of-function mutations that affect the rapid upstroke of the AP. In human embryonic stem cell (ESC)-derived cardiomyocytes, the relative contribution of I_{Na} to phase 0 of the AP is a matter of debate, with upstroke velocities of ≈8 V/s typically detected in human ESC cardiomyocytes [13-16] compared with ≈200 V/s in adult cardiomyocytes [17]. In human iPSC-derived cardiomyocytes (hiPSC-CMs), similar low upstroke velocities have also been reported [18-20]. Although mouse (m)PSC-CMs show an increase in I_{Na} and upstroke velocity during prolonged in vitro differentiation [21-23], the latter is still smaller than that observed in isolated primary adult mouse cardiomyocytes [8]. Therefore, it remains uncertain whether PSC-CMs can recapitulate the electrophysiological features of Na^+ channel loss-of-function mutations.

In this study, we generated iPSC lines from Scn5a-het mice and from wild-type littermates and derived functional cardiomyocytes from them. In addition, the mouse (m)ESC line used to introduce the *Scn5a*-1798insD mutation into the mice, as well as the parental (Scn5a-wt) control mESC line, were differentiated into cardiomyocytes. The biophysical properties of the Na^+ channel and AP characteristics in cardiomyocytes derived from these two PSC sources were examined and compared with those observed in cardiomyocytes isolated from Scn5a-wt and -het mice that were described previously [8,9]. Both in vitro Scn5a-het models recapitulated the electrophysiological phenotype observed in the corresponding primary adult cardiomyocytes. Finally, to ascertain whether some of the electrophysiological features underlying LQT3 and BrS could also be detected in human cardiomyocytes, we generated an hiPSC line from a patient carrying the *SCN5A*-1795insD variant. Cardiomyocytes derived from these cells also displayed the I_{Na} and AP properties of this cardiac Na^+ channelopathy. Collectively, these results demonstrate the utility of PSCs in modeling even complex ion channel disorders.

Methods

An expanded Methods section is available in the Supplemental Methods.

Mouse (m)iPSCs and hiPSCs were generated essentially as described previously [24-26] by either retroviral or lentiviral transduction of vectors encoding Oct4, Sox2, Klf4, and c-Myc. The undifferentiated PSC lines were maintained by standard procedures [27,28]. Teratomas were generated by injecting undifferentiated iPSCs into nonobese diabetic severe combined immunodeficiency (NOD-SCID) mice. mPSCs were differentiated in vitro as embryoid bodies (EBs) using a “hanging drop” protocol [27], whereas hiPSCs were induced to differentiate to cardiomyocytes by coculture on visceral endoderm-like (END-2) cells as described previously [28,29]. Immunofluorescence and gene expression analyses were performed as

described previously [28,30]. PSC-CMs were isolated from differentiated EBs by enzymatic dissociation and the electrophysiological recordings obtained by the use of either ruptured or perforated patch-clamp techniques. Results are expressed as mean±SEM. Comparisons were made by use of an unpaired Student *t* test, one-way ANOVA, or two-way repeated measures ANOVA, followed by a Holm-Sidak test for post hoc analysis. Values of $P<0.05$ were considered statistically significant. Statistical analyses were performed with SigmaStat software.

Results

Generation and Characterization of Scn5a-wt and -het mPSC Lines

The mESC line in which one allele of the *Scn5a* locus was modified to contain the 1798insD mutation and the corresponding mutant mouse used to generate the miPSC lines have been described previously [7,8]. Fibroblasts cultured from Scn5a-wt and -het littermates were reprogrammed to generate the corresponding miPSC lines. Several independent clones for each genotype were obtained from both adult tail-tip and embryonic fibroblasts. The 1798insD heterozygous mutation in the *Scn5a* locus was confirmed to be present in the Scn5a-het mESCs and miPSCs but not in the wild-type lines (Supplemental Figure 1).

The miPSC lines resembled mESCs in terms of morphology and expression of ESC-associated markers (Oct4, Nanog, and SSEA-1; Figure 1A) and had reactivated endogenous pluripotency genes (*Oct4, Nanog, Sox2, Rex1*, and *ECat1*; Figure 1B). Furthermore, the miPSCs when differentiated in vitro expressed the mesoderm marker α-smooth muscle actin, the endoderm marker Sox17, and the ectoderm marker glial fibrillary acidic protein (Figure 1C). Additionally, undifferentiated miPSCs injected into immunocompromised NOD-SCID mice formed teratomas containing cell derivatives of the 3 germ layers (Figure 1D and 1E). Collectively, these results indicate that the adult somatic cells were reprogrammed to a pluripotent state.

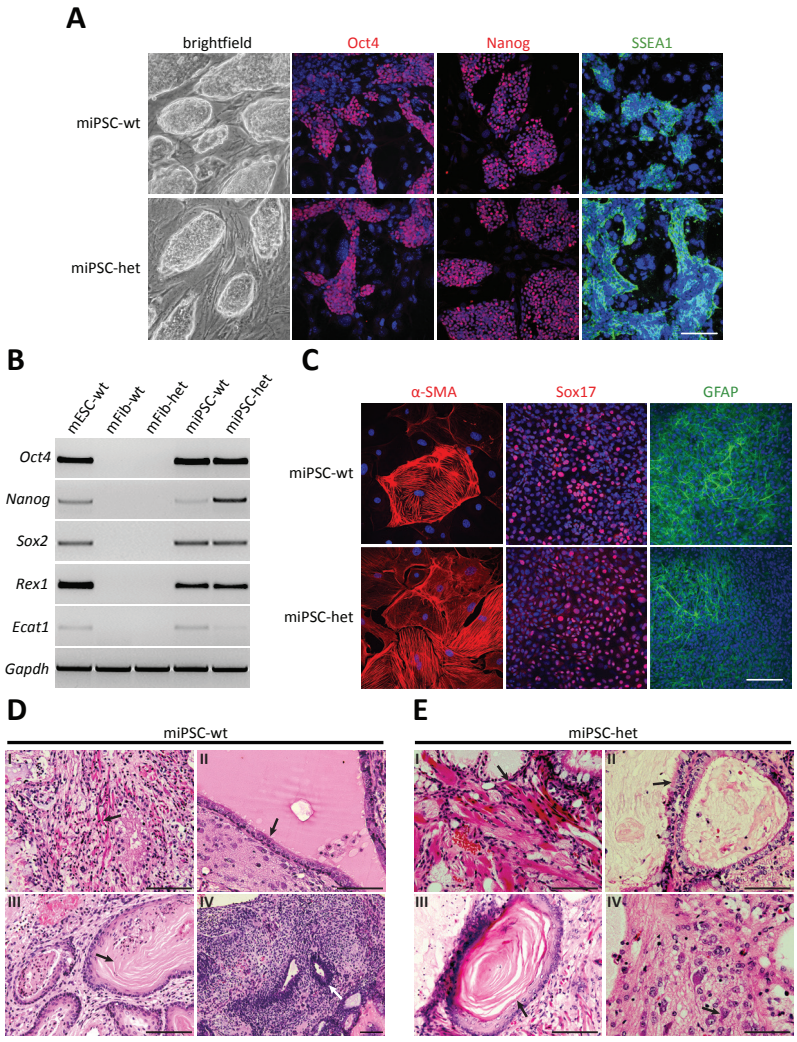

Figure 1. Characterization of control and Scn5a-het mouse induced pluripotent stem cell (miPSC) lines

A, Shown from left to right are bright-field images (original magnification ×125) and immunofluorescent images for Oct4, Nanog, and SSEA-1 of Scn5a-wt (top) and Scn5a-het (bottom) miPSCs. Nuclei were stained with DAPI (blue). **B**, Reverse transcriptase-polymerase chain reaction analysis of endogenous *Oct4, Nanog, Sox2, Rex1*, and *Ecat1* expression in Scn5a-wt and -het mouse fibroblasts (mFib) and miPSCs. Scn5a-wt mESCs were used as a positive control, and *Gapdh* was used as a loading control. **C**, Immunofluorescent analysis of embryoid bodies from Scn5a-wt (top) and Scn5a-het (bottom) miPSCs for the differentiation markers α-smooth muscle actin (α-SMA), Sox17, and glial fibrillary acidic protein (GFAP). Nuclei were stained with DAPI. **D**, Teratoma derived from Scn5a-wt miPSCs comprising cell types from all 3 germ layers. Arrows indicate striated muscle fibers (I), thyroid-like follicles (II), keratinized stratified squamous epithelium (III), and neural rosettes (IV). **E**, Teratoma derived from Scn5a-het miPSCs comprising cell types from all 3 germ layers. Arrows indicate striated muscle fibers (I), pseudostratified ciliated columnar epithelium (II), keratinized stratified squamous epithelium (III), and neurons (IV). Scale bars represent 100 µm. wt indicates $Scn5a^{+/+}$; het, $Scn5a^{1798insD/+}$.

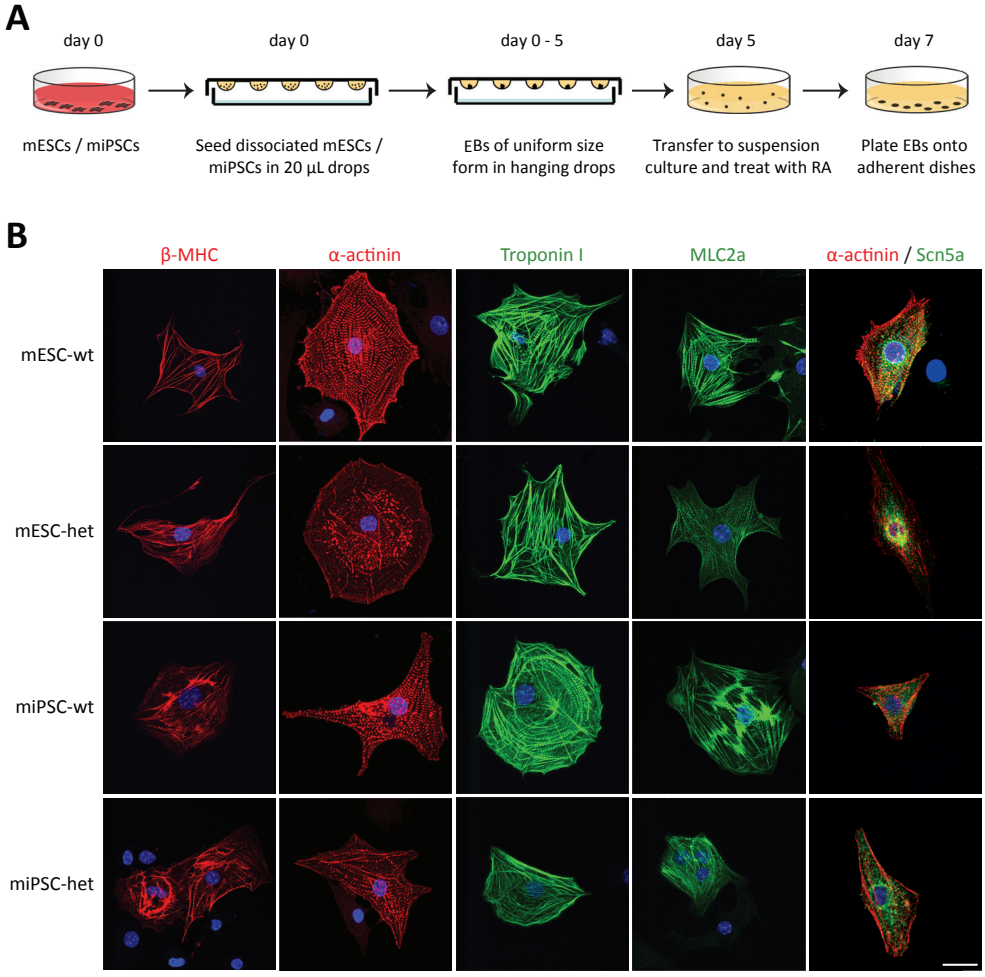

Figure 2. Differentiation of mouse embryonic stem cells (mESCs) and mouse induced pluripotent stem cells (miPSCs) to cardiomyocytes

A, Schematic detailing the procedure to differentiate mESCs and miPSCs to cardiomyocytes. EBs indicates embryoid bodies; RA, retinoic acid. **B**, Immunofluorescent images of the cardiac markers β-myosin heavy chain (β-MHC), α-actinin, troponin I, myosin light chain 2 atrial isoform (MLC2a), and Scn5a in cardiomyocytes derived from Scn5a-wt and Scn5a-het mESCs and miPSCs. All cells were costained with the nuclear dye DAPI (blue). Scale bars represent 25 µm. wt indicates *Scn5a*$^{+/+}$; het, *Scn5a*$^{1798insD/+}$.

Scn5a-wt and -het mPSCs Differentiate Into Cardiomyocytes

Scn5a-wt and -het mESCs and miPSCs were differentiated to cardiomyocytes in EBs (Figure 2A) [27,31]. One day after EBs were transferred to adherent culture (day 8 of differentiation), spontaneously contracting foci were apparent (Supplemental Movie 1). By day 10 of differentiation, 75 % to 90 % of mESC- and miPSC-derived EBs contained spontaneously contracting regions, indicating comparable cardiomyocyte differentiation potentials (Supplemental Figure 2A). Additionally, no significant difference in the spontaneous beating

rate was observed between Scn5a-wt and -het mPSC-EBs (Supplemental Figure 2B). Gene expression profiling of mESC- and miPSC-derived EBs revealed a similar differentiation pattern into mesodermal and cardiac cells for all 4 lines, including expression of *Scn5a* from day 3 of differentiation (Supplemental Figure 3). Cardiomyocytes isolated from Scn5a-wt and -het mESCs and miPSCs displayed organized cross-striations resembling sarcomeres that were positive for β-myosin heavy chain, α-sarcomeric actinin, troponin I, and myosin light chain 2A (Figure 2B). Similar to the findings of others [32], α-actinin-positive cells from both Scn5a-wt and-het mPSC-CMs also displayed Na^+ channel staining (Figure 2B).

Scn5a-het mESC-CMs and miPSC-CMs Display Reduced I_{Na}

I_{Na} electrophysiological properties were studied with the patch-clamp technique in cardiomyocytes derived from mESCs and miPSCs. As others have reported [21-23,32], we observed an increase in I_{Na} in mPSC-CMs with prolonged culture, reaching a plateau at around day 17 of differentiation (Supplemental Figure 4A and 4B). Therefore, only cardiomyocytes after 17 or 18 days of differentiation were analyzed further. The capacitance was similar for all mPSC-CMs and did not change over time (Table 1 and Supplemental Figure 4A and 4B). Typical examples of I_{Na} recordings obtained from Scn5a-wt and -het mPSC-CMs are shown in Figure 3A and 3B. Average I_{Na} density was significantly reduced in Scn5a-het cardiomyocytes derived from both groups compared with their respective control cells (Figure 3C and 3D). At the membrane potential of −30 mV, I_{Na} density was reduced by 44 % in Scn5a-het mESC-CMs and by 48 % in Scn5a-het miPSC-CMs (Figure 3E and 3F and Table 1), mirroring similar reductions observed in primary cardiomyocytes isolated from 129P2 Scn5a-het mice (54 %) [8]. Scn5a-wt and -het miPSC lines derived from mouse embryonic fibroblasts also displayed similar I_{Na} density differences in their corresponding cardiomyocytes (Supplemental Figure 4C), indicating that the electrophysiological phenotype was conserved between different miPSC clones independently of whether they were obtained by reprogramming tail-tip fibroblasts or embryonic fibroblasts.

As we observed previously in primary cardiomyocytes isolated from the Scn5a-het mice [8], voltage dependence of activation and inactivation parameters (half-maximal voltage [$V_{1/2}$] and slope factor [k]) did not differ significantly between either Scn5a-wt and-het mESC-CMs or Scn5a-wt and-het miPSC-CMs (Figure 4A–4D and Table 1). In addition, fast and slow time constants (τ_f and τ_s) of recovery from inactivation were comparable for Scn5a-wt and -het cardiomyocytes in both groups (Figure 4E and 4F and Table 1). The fraction of channels (A) entering the slow inactivated state and the rate of development of slow inactivation (τ) also did not differ between Scn5a-wt and -het cardiomyocytes derived from either PSC source (Figure 4G and 4H and Table 1).

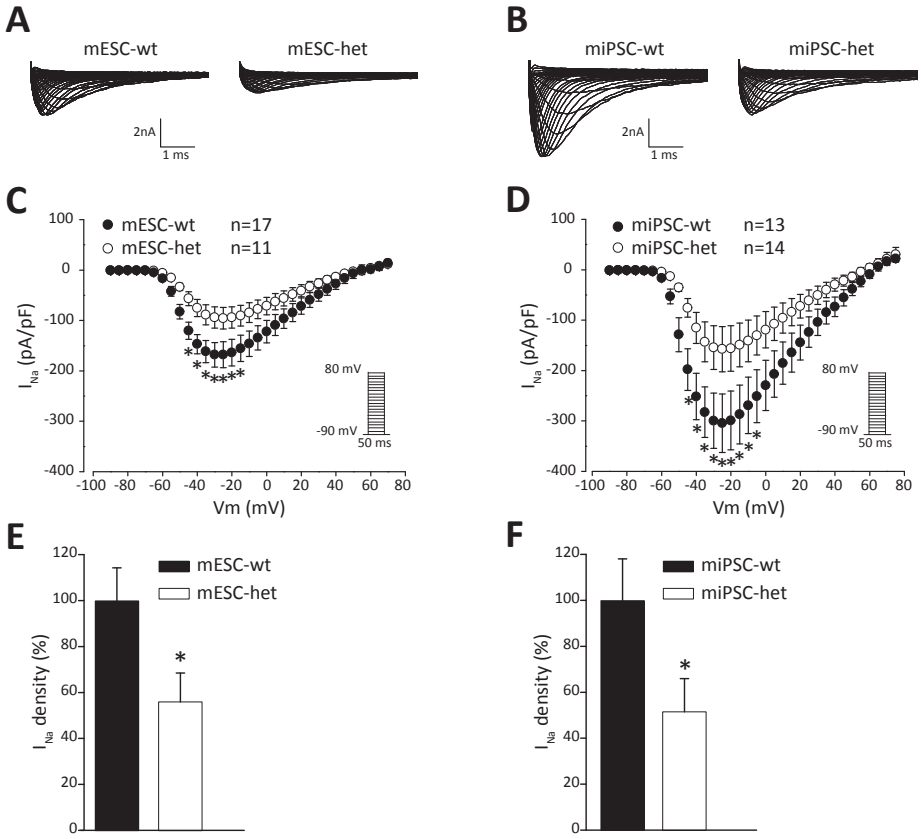

Figure 3. Na^+ current (I_{Na}) densities in cardiomyocytes derived from Scn5a-wt and Scn5a-het mouse embryonic stem cells (mESCs) and mouse induced pluripotent stem cells (miPSCs)

A and **B**, Examples of I_{Na} traces recorded from Scn5a-wt and Scn5a-het cardiomyocytes derived from mESCs (A) and miPSCs (B). **C** and **D**, Average current-voltage relationships for Scn5a-wt and Scn5a-het cardiomyocytes derived from mESCs (C) and miPSCs (D). Voltage protocols shown as insets. **E** and **F**, I_{Na} density, measured at −30 mV, in Scn5a-het cardiomyocytes relative to Scn5a-wt cardiomyocytes derived from mESCs (E) and miPSCs (F) expressed as a percentage. *Statistical significance (P<0.05, two-way repeated measures ANOVA [C and D] or t test [E and F]). wt indicates *Scn5a*$^{+/+}$; het, *Scn5a*$^{1798insD/+}$.

Table 1. Na^+ Channel Biophysical Properties in Cardiomyocytes Derived From Scn5a-wt and Scn5a-het Mouse Embryonic Stem Cells and Mouse Induced Pluripotent Stem Cells

	mESC-wt	n	mESC-het	n	miPSC-wt	n	miPSC-het	n
Cell capacitance, pF	22.2±2.0	17	19.7±3.0	11	16.4±1.6	13	19.3±1.5	14
Current density								
I_{Na}, pA/pF	−168.1±24.2	17	−94.1±21.1*	11	−299.6±54.7	13	−154.5±43.4†	14
Activation								
$V_{1/2}$, mV	−45.9±1.4	17	−42.5±1.6	11	−43.7±1.3	13	−42.6±1.3	14
k, mV	5.8±0.3		6.6±0.4		5.6±0.4		6.0±0.2	
Inactivation								
$V_{1/2}$, mV	−90.8±1.7	14	−90.6±2.5	9	−91.1±0.7	11	−91.6±0.9	12
k, mV	−6.2±0.2		−6.4±0.2		−6.2±0.2		−5.8±0.2	
Recovery from inactivation								
τ_f, ms	57.2±9.5	10	61.1±8.6	8	51.6±4.0	11	54.3±8.3	8
τ_s, ms	378.4±78.0		374.1±78.2		478.1±83.9		420.6±104.4	
Slow inactivation								
A	0.27±0.02	9	0.28±0.03	7	0.28±0.03	9	0.29±0.04	8
τ, ms	1065.8±161.3		904.3±202.5		1158.1±136.4		1405.3±192.0	

mESC indicates mouse embryonic stem cell; wt, *Scn5a*$^{+/+}$; het, *Scn5a*$^{1798insD/+}$; miPSC, mouse induced pluripotent stem cells; n, number of myocytes; I_{Na}, Na^+ current density measured at −30 mV; $V_{1/2}$, voltage of half-maximal (in)activation; k, slope factor of voltage dependence of (in)activation; τ_f and τ_s, fast and slow time constants of recovery from inactivation; A, fraction of channels that enter the slow inactivated state; and τ, time constant for development of slow inactivation. Values are mean±SEM. Statistical comparisons were performed with the *t* test between either mESC-wt and-het or miPSC-wt and-het.

* *P*=0.04 vs mESC-wt.

† *P*=0.04 vs miPSC-wt.

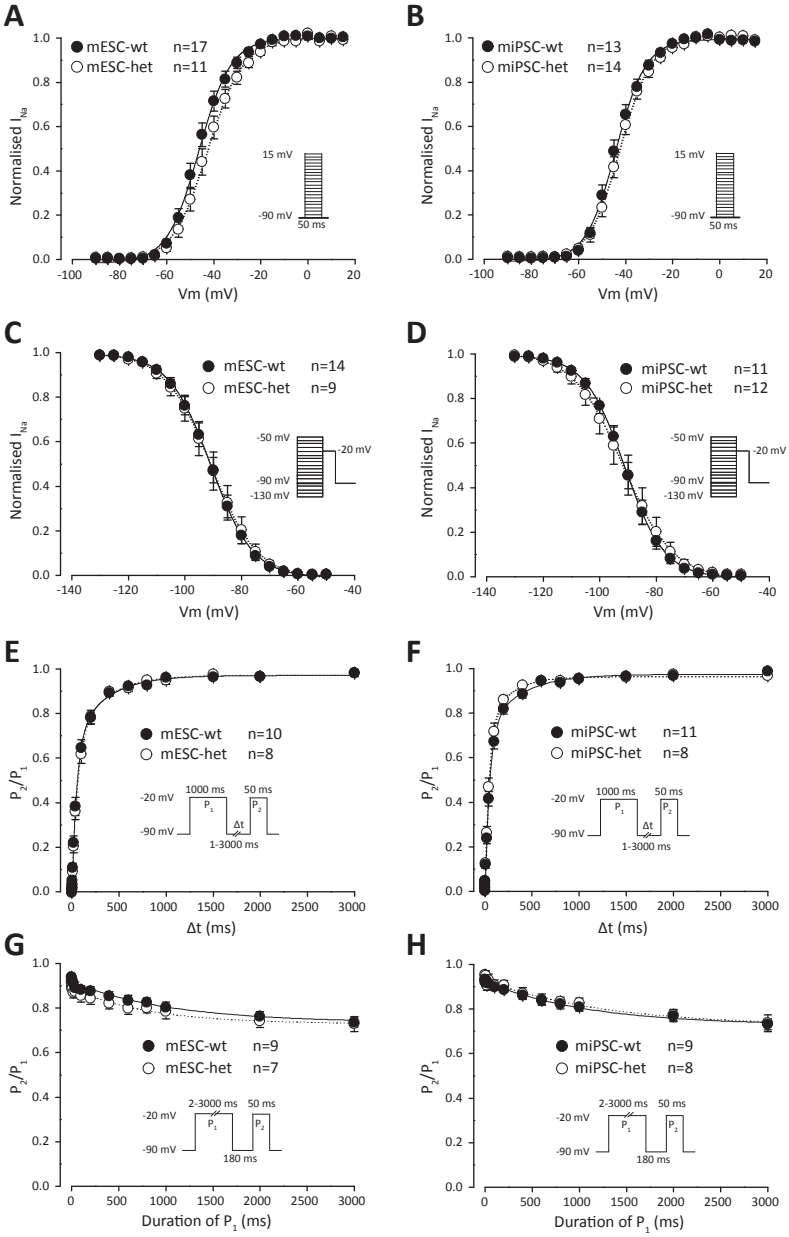

Figure 4. Na^+ current gating properties in cardiomyocytes derived from Scn5a-wt and Scn5a-het mouse embryonic stem cells (mESCs) and mouse induced pluripotent stem cells (miPSCs)
A through **H**, Average voltage dependence of activation (**A** and **B**), voltage dependence of inactivation (**C** and **D**), recovery from inactivation (**E** and **F**), and development of slow inactivation (**G** and **H**) for Scn5a-wt and Scn5a-het cardiomyocytes derived from mESCs and miPSCs. Voltage protocols are shown as insets. Data are summarized in Table 1. wt indicates *Scn5a*$^{+/+}$; het, *Scn5a*$^{1798insD/+}$.

Scn5a-het mESC-CMs and miPSC-CMs Exhibit a Larger Persistent I_{Na}

Persistent I_{Na} was measured as a 30 µmol/L tetrodotoxin-sensitive current either during a descending voltage ramp protocol or at the end of a 200-millisecond test pulse to −30 mV. Representative examples of traces obtained from Scn5a-wt and -het mPSC-CMs illustrating the difference in I_{Na} after application of tetrodotoxin are shown (Figure 5A and 5B and Supplemental Figure 5A and 5B). In both Scn5a-het mESC- and miPSC-CMs, the persistent I_{Na} density was significantly increased compared with their respective controls (Figure 5C and 5D and Supplemental Figure 5C–5E). This is in agreement with the increased persistent I_{Na} density we reported in adult cardiomyocytes isolated from Scn5a-het mice [9].

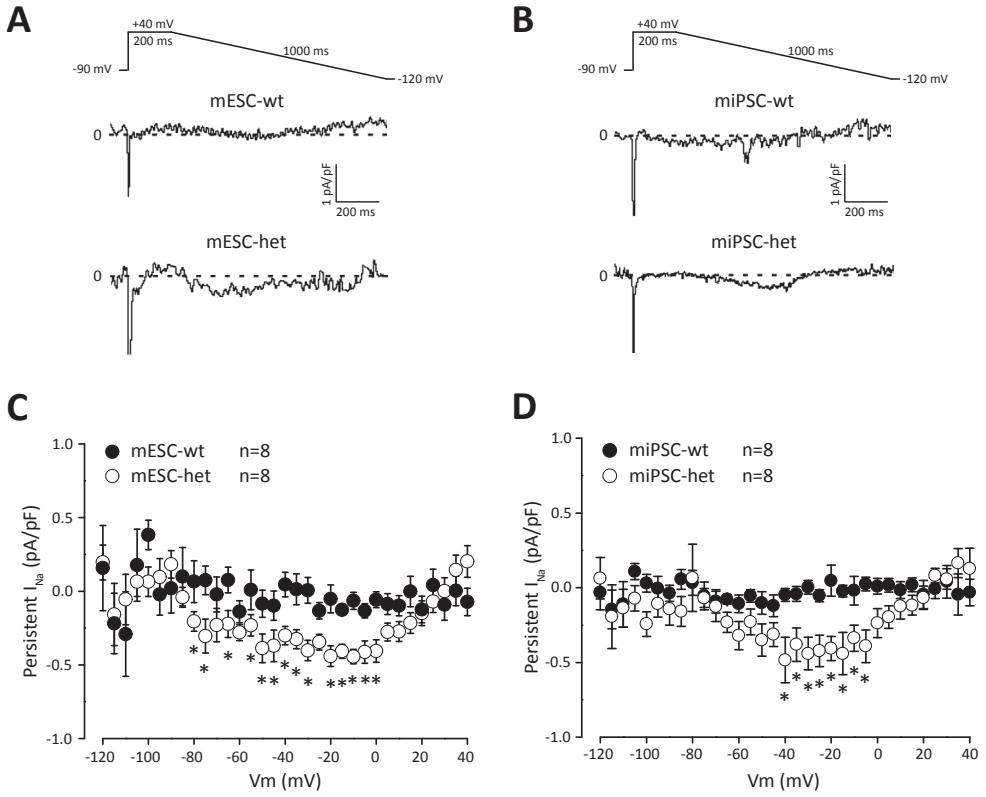

Figure 5. Persistent Na⁺ current (I_{Na}) measurements in cardiomyocytes derived from Scn5a-wt and Scn5a-het mouse embryonic stem cells (mESCs) and mouse induced pluripotent stem cells (miPSCs)
A and **B**, Persistent I_{Na} traces obtained by subtraction of the current before and after application of 30 µmol/L tetrodotoxin in Scn5a-wt (top) and Scn5a-het (bottom) cardiomyocytes derived from mESCs (A) and miPSCs (B). Voltage protocols are shown above the traces. **C** and **D**, Average values for persistent I_{Na} density in mESC-CMs (C) and miPSC-CMs (D). *Statistical significance (P<0.05, two-way repeated measures ANOVA). wt indicates *Scn5a*$^{+/+}$; het, *Scn5a*$^{1798insD/+}$.

Scn5a-het mESC-CMs and miPSC-CMs Exhibit a Reduced Upstroke Velocity and a Prolonged AP

In our previous studies [8], adult cardiomyocytes isolated from *Scn5a*$^{1798insD/+}$ mice were shown to have prolonged APD and reduced upstroke velocity compared with wild-type cardiomyocytes. To determine whether this was captured by mESC- and miPSC-CMs, APs were measured. Representative examples of APs and upstroke velocities from Scn5a-wt and-het mPSC-CMs, measured at 6 Hz, are shown in Figure 6A and 6B. V_{max} was significantly smaller and APD at 90 % repolarization (APD_{90}) was significantly prolonged in Scn5a-het cardiomyocytes derived from both mESCs and miPSCs compared with cardiomyocytes from the corresponding controls (Figure 6C and 6D and Table 2). No significant differences in resting membrane potential (RMP) and APD at 20 % and 50 % repolarization (APD_{20} and APD_{50}) were observed between Scn5a-wt and-het cardiomyocytes in both groups, although Scn5a-het mESC-CMs showed a reduction in AP amplitude compared with Scn5a-wt mESC-CMs (Figure 6C and 6D and Table 2). This reduction is likely due to the low V_{max} observed in the Scn5a-het mESC-CMs. Overall, the miPSC-CMs had a more hyperpolarized RMP and higher V_{max} than the mESC-CMs. The higher V_{max} is also in line with the observed larger I_{Na} density (Figure 3C and 3D). At slower pacing frequencies, the differences in V_{max} and APD_{90} remained in both mESC- and miPSC-CMs, although the APD_{90} was no longer significantly prolonged in the mESC-CMs because of the relatively large variability between individual mESC-CMs (Supplemental Figure 6).

Table 2. Action Potential Characteristics in Cardiomyocytes Derived From Scn5a-wt and Scn5a-het Mouse Embryonic Stem Cells and Mouse Induced Pluripotent Stem Cells

	mESC-wt (n=12)	**mESC-het** (n=8)	*P*	**miPSC-wt** (n=11)	**miPSC-het** (n=10)	*P*
RMP, mV	−71.6±1.0	−69.9±0.7		−77.4±1.4	−76.9±2.1	
APA, mV	104.1±4.7	85.8±2.8	0.006	112.2±2.6	110.4±1.6	
V_{max}, V/s	119.5±14.8	57.1±12.1	0.006	272.3±23.6	133.5±16.4	7×10^{-5}
APD_{20}, ms	9.4±2.2	15.3±4.4		7.6±2.2	12.9±2.6	
APD_{50}, ms	19.2±4.2	26.6±7.2		20.4±3.8	28.9±5.1	
APD_{90}, ms	52.4±7.5	76.2±8.2	0.04	70.5±6.7	92.7±9.0	0.04

mESC indicates mouse embryonic stem cell; wt, *Scn5a*$^{+/+}$; het, *Scn5a*$^{1798insD/+}$; miPSC, mouse induced pluripotent stem cells; n, number of myocytes; RMP, resting membrane potential; APA, action potential amplitude; V_{max}, maximal upstroke velocity; and $APD_{20,}$ APD_{50}, and APD_{90}, action potential duration at 20%, 50%, and 90% repolarization, respectively. Values are mean±SEM. Statistical comparisons were performed with the *t* test between either mESC-wt and-het or miPSC-wt and-het.

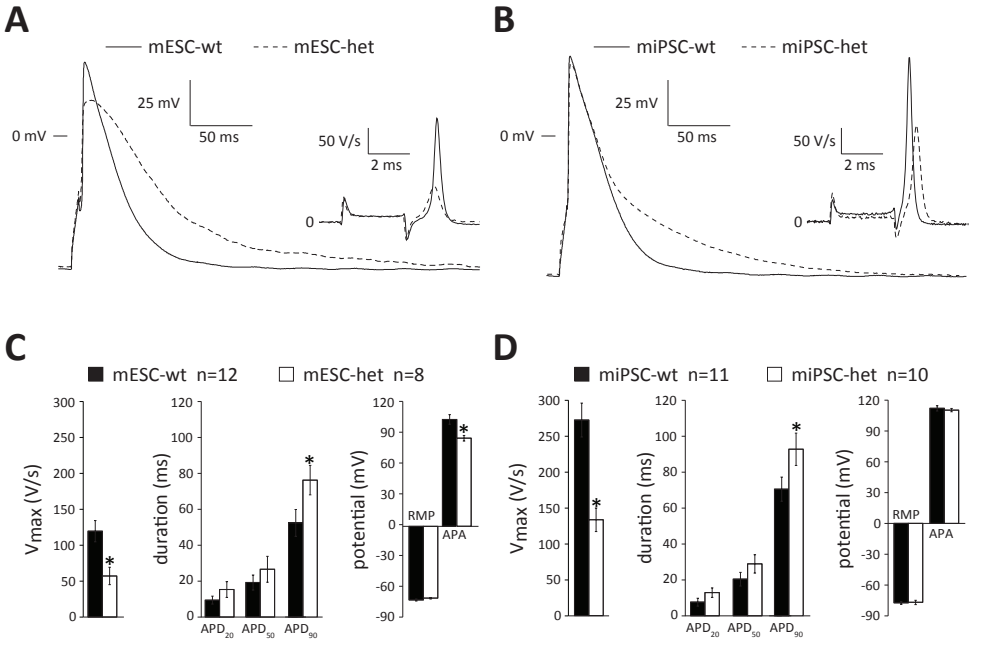

Figure 6. Action potential (AP) characteristics of cardiomyocytes derived from Scn5a-wt and Scn5a-het mouse embryonic stem cells (mESCs) and mouse induced pluripotent stem cells (miPSCs)
A and **B**, Examples of AP and upstroke velocity (V_{max}, inset) measured in Scn5a-wt and Scn5a-het cardiomyocytes derived from mESCs (A) and miPSCs (B). **C** and **D**, Average data at 6 Hz for V_{max}, AP duration at 20 %, 50 %, and 90 % repolarization (APD_{20}, APD_{50}, and APD_{90}), resting membrane potential (RMP), and AP amplitude (APA) in Scn5a-wt and Scn5a-het cardiomyocytes derived from mESCs (C) and miPSCs (D). *Statistical significance (P<0.05, t test). Data are summarized in Table 2. wt indicates *Scn5a*$^{+/+}$; het, *Scn5a*$^{1798insD/+}$.

SCN5A-het hiPSC-CMs Have Reduced I_{Na} Density and Prolonged AP

To determine whether cardiomyocytes derived from a human iPSC line carrying the *SCN5A*-1795insD mutation (SCN5A-het) also had reduced I_{Na} and a longer AP compared with SCN5A-wt hiPSC-CMs, we reprogrammed dermal fibroblasts from a patient with the mutation and from an unaffected individual. Sequencing of genomic DNA confirmed heterozygosity for the *SCN5A* c.5387_5389insTGA mutation in the SCN5A-het hiPSCs, resulting in the insertion of aspartic acid after tyrosine 1795 (1795insD; Figure 7A). There was no TGA insertion at the corresponding position in the SCN5A-wt hiPSCs (Supplemental Figure 7A). Both hiPSC lines maintained a normal karyotype, showed characteristic human ESC morphology, and expressed the ESC markers OCT4, NANOG, TRA-1-81, and SSEA4 (Figure 7B and 7C and Supplemental Figure 7B and 7C). Additionally, EB differentiation of the hiPSCs demonstrated that the cells could generate derivatives of the 3 embryonic germ layers based on expression of the markers α-smooth muscle actin, SOX17, and glial fibrillary acidic protein (Figure 7D and Supplemental Figure 7D).

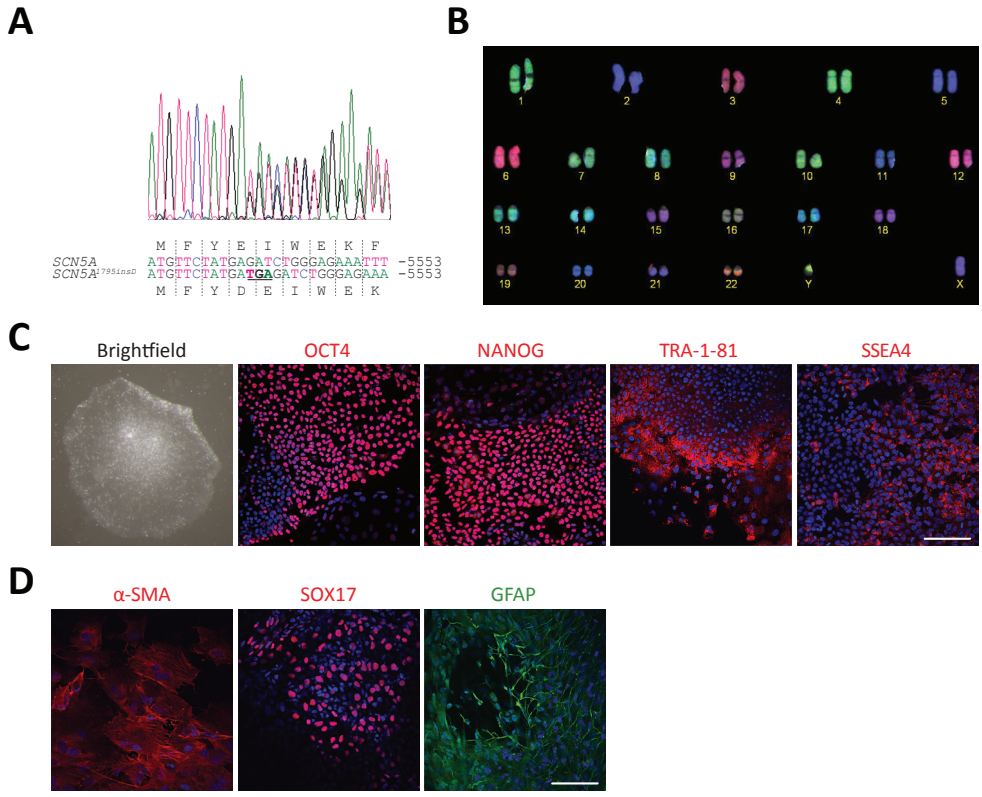

Figure 7. Characterization of SCN5A-het human induced pluripotent stem cells (hiPSCs)
A, Sequence analysis of *SCN5A* in SCN5A-het hiPSCs showing the insertion of the nucleotides TGA in 1 allele, resulting in the addition of aspartic acid (D) at position 1795 of the SCN5A protein. **B**, Karyogram generated by combined binary ratio labeling fluorescence in situ hybridisation (COBRA-FISH) of SCN5A-het hiPSCs showing a normal 46XY karyotype. **C**, Shown from left to right are a bright-field image (original magnification ×16) of and immunofluorescent images for OCT3/4, NANOG, TRA-1-81, and SSEA4 in SCN5A-het hiPSCs. Nuclei were stained with DAPI (blue). **D**, Immunostaining of embryoid bodies from SCN5A-het hiPSCs for the differentiation markers α-smooth muscle actin (α-SMA), SOX17, and glial fibrillary acidic protein (GFAP). Nuclei were stained with DAPI. Scale bars in C and D represent 100 µm.

To differentiate the SCN5A-wt and-het hiPSCs to cardiomyocytes, the cells were cocultured with END-2 cells, and rhythmically contracting areas started to appear after 6 days. At day 12 of differentiation, the spontaneous beating frequency was not significantly different between the SCN5A-wt and-het hiPSC-CMs (Supplemental Figure 7A and Supplemental Movie 2). Immunodetection with antibodies recognizing β-myosin heavy chain, α-actinin, troponin I, and myosin light chain 2A confirmed the presence of cardiomyocytes with characteristic cardiac muscle striations within these beating areas (Figure 8A).

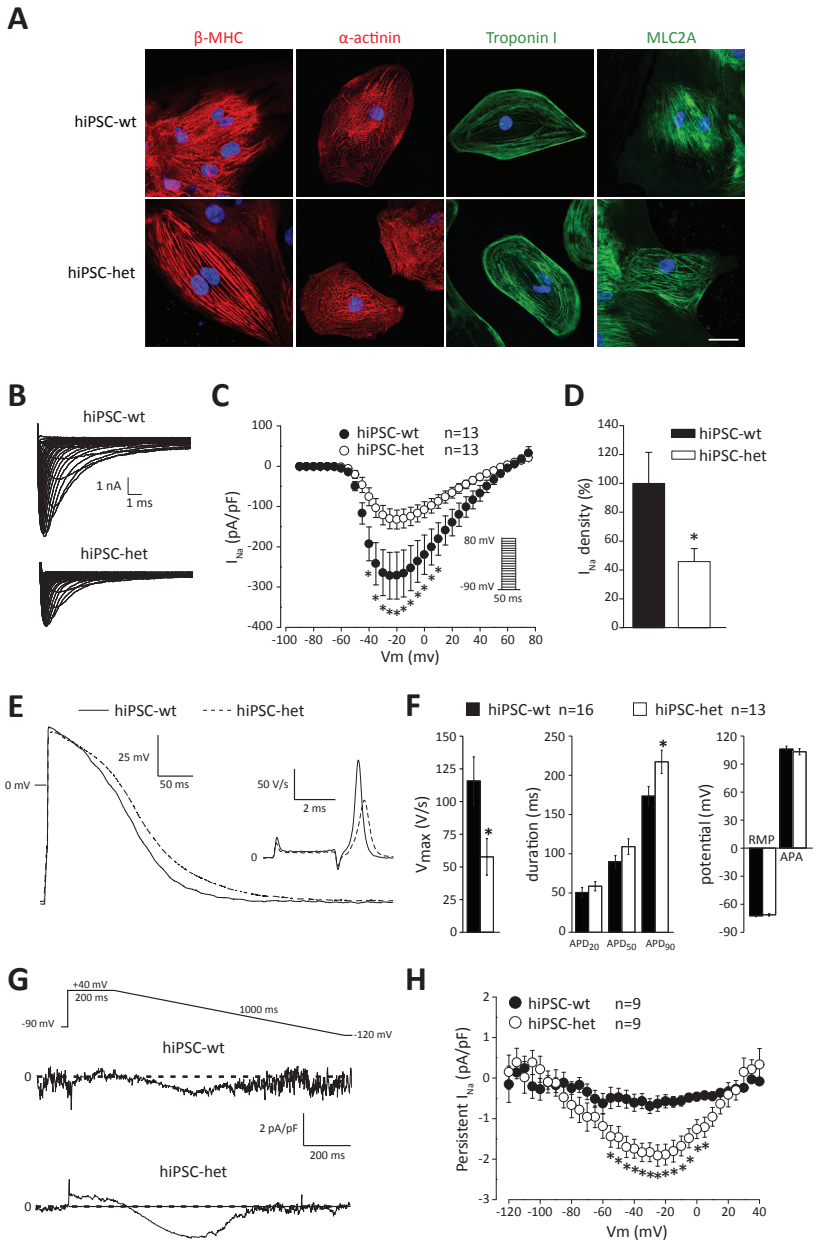

Figure 8. Characterization of cardiomyocytes derived from SCN5A-wt and SCN5A-het human induced pluripotent stem cells (hiPSCs)

A, Immunofluorescent images of the cardiac markers β-myosin heavy chain (β-MHC), α-actinin, troponin I, and myosin light chain 2 atrial isoform (MLC2A) in SCN5A-wt (top) and SCN5A-het (bottom) hiPSC cardiomyocytes (CMs). All cells were costained with the nuclear dye DAPI (blue). Scale bars represent 25 µm. **B**, Examples of Na^+ current (I_{Na}) traces recorded in SCN5A-wt (top) and SCN5A-het (bottom)

hiPSCs-CMs. **C**, Average current-voltage relationships for SCN5A-wt and SCN5A-het hiPSC-CMs. The capacitance (Cm) was 36.0±3.3 pF in the SCN5A-wt and 31.7±3.2 pF in the SCN5A-het cardiomyocytes. **D**, I_{Na} density, measured at −30 mV, in SCN5A-het hiPSC-CMs (−121.4±23.8 pA/pF) relative to SCN5A-wt hiPSC-CMs (−264.4±57.0 pA/pF) expressed as a percentage. **E**, Examples of action potential (AP) and upstroke velocity (V_{max}, inset) recorded in SCN5A-wt and SCN5A-het hiPSC-CMs. **F**, Average data at 1 Hz for V_{max}, AP duration at 20 %, 50 %, and 90 % repolarization (APD_{20}, APD_{50}, and APD_{90}), resting membrane potential (RMP), and AP amplitude (APA) in SCN5A-wt and SCN5A-het hiPSC-CMs. **G**, Persistent I_{Na} traces obtained by subtraction of the current before and after application of 30 µmol/L tetrodotoxin in SCN5A-wt (top) and SCN5A-het (bottom) hiPSCs-CMs. The voltage protocol is shown above the traces. **H**, Average values for persistent I_{Na} density in hiPSCs-CMs. *Statistical significance (P<0.05, two-way repeated measures ANOVA [C and H] or t test [D and F]). wt indicates *SCN5A*$^{+/+}$; het, *SCN5A*$^{1795insD/+}$.

Representative examples of I_{Na} recorded from SCN5A-wt and -het hiPSC-CMs are shown in Figure 8B. Similar to our findings in mPSC-CMs (Figure 3C and 3D), average I_{Na} density was significantly decreased in SCN5A-het hiPSC-CMs (Figure 8C), with peak I_{Na} density at −30 mV being 46 % of that observed in control hiPSC-CMs (Figure 8D and Table 3). Typical examples of APs and upstroke velocities in SCN5A-wt and -het hiPSC-CMs paced at 1 Hz are shown in Figure 8E. Similar to Scn5a-het mPSC-CMs, SCN5A-het hiPSC-CMs had a significantly smaller V_{max} and longer APD_{90} compared with the control cardiomyocytes (Figure 8F and Table 3). No differences in APD_{20}, APD_{50}, RMP, and AP amplitude were detected between the 2 groups (Figure 8F and Table 3). The differences in V_{max} and APD_{90} also persisted at faster pacing frequencies (Supplemental Figure 8B). Examples of persistent I_{Na} measured during a descending ramp protocol are shown in Figure 8G. As observed in the Scn5a-het mPSC-CMs (Figure 5), the persistent I_{Na} was also significantly larger in the SCN5A-het hiPSC-CMs compared with the SCN5A-wt cardiomyocytes (Figure 8H).

Table 3. Action Potential Characteristics in Cardiomyocytes Derived From SCN5A-wt and SCN5A-het Human Induced Pluripotent Stem Cells

	hiPSC-wt (n=16)	**hiPSC-het** (n=13)
RMP, mV	−72.4±0.9	−71.3±1.3
APA, mV	106.0±3.2	103.1±3.2
V_{max}, V/s	115.7±18.4	57.6±14.0*
APD_{20}, ms	50.7±6.2	58.7±5.9
APD_{50}, ms	89.8±7.9	109.0±10.1
APD_{90}, ms	173.5±12.2	217.2±14.9†

hiPSC indicates human induced pluripotent stem cell; wt, *SCN5A*$^{+/+}$ het, *SCN5A*$^{1795insD/+}$; n, number of myocytes; RMP, resting membrane potential; APA, action potential amplitude; V_{max}, maximal upstroke velocity; and APD_{20}, APD_{50}, and APD_{90}, action potential duration at 20 %, 50 %, and 90 % repolarization, respectively. Values are mean±SEM. Statistical comparisons were performed with the t test.
* P=0.02 vs hiPSC-wt.
† P=0.03 vs hiPSC-wt.

Discussion

Recent advances in the PSC field have created unprecedented opportunities to study cardiac disease development in vitro and to establish novel platforms for drug discovery, either to prevent or to reverse disease progression. Several reports have already confirmed the ability of iPSC-CMs to model K^+, Ca^{2+}, and Na^+ gain-of-function mutations [18,19,32-34]. Here, we demonstrate that cardiomyocytes derived from both ESCs and iPSCs can model a combined loss- and gain-of-function Na^+ channel mutation that is conserved between humans and mice [7].

We chose to investigate this *Scn5a* mutation originally in mPSC-CMs for several reasons. First, it has previously been established that although mESC-CMs do not initially express any detectable I_{Na}, this current and the related upstroke velocity values increase as the cardiomyocytes mature in vitro, with phase 0 of the AP becoming Na^+ dependent [21]. Second, the *Scn5a*$^{1798insD/+}$ mouse has been extensively characterized [7,8], therefore offering the opportunity to compare the biophysical properties of the Na^+ channel in primary cardiomyocytes freshly isolated from the mice with cardiomyocytes either from the ESCs used to generate the mutant mouse or from the miPSCs derived by reprogramming the corresponding fibroblasts. This direct comparison is not possible with human PSC cardiac disease models because sufficient numbers of human ventricular cardiomyocytes cannot be obtained from patients. Finally, by comparing the cardiomyocytes from Scn5a-het mESCs and those from the unmodified mESC line, we could confirm that the observed electrophysiological differences were due to the mutation. Electrophysiological changes similar to those present between the Scn5a-wt and-het mESC-CMs were also detected in both mouse and human iPSCs, suggesting that the reprogramming method did not influence the electrophysiological phenotype.

As observed in cardiomyocytes isolated from the postnatal Scn5a-het mouse [7,8], Scn5a-het mPSC-CMs displayed a significant reduction in I_{Na} density and upstroke velocity. These cells also presented an increased persistent I_{Na} leading to a longer AP compared with control cardiomyocytes, although because of the reduced AP amplitude in the Scn5a-het mESC-CMs, differences in K^+ current activation might also contribute here to the prolonged APD. In addition, no significant changes were observed in the voltage dependence of (in)activation, recovery from inactivation, or development of slow inactivation. This is in contrast to previous findings on the biophysical properties of the 1795insD mutation in HEK 293 cells in which the mutation did not affect I_{Na} density but altered the voltage dependence of inactivation and enhanced slow inactivation [10]. A possible reason for this discrepancy is that only the SCN5A-1795insD channel was expressed in these cells, rather than coexpression of both the wild-type and mutant channels, as occurs in primary and PSC-derived cardiomyocytes. The presence of wild-type SCN5A might compensate for small changes in current kinetics caused by the 1795insD mutation. Additionally, only the β1-subunit was coexpressed with SCN5A.

In cardiomyocytes, four β-subunits (and other Na^+ channel-interacting proteins) associate with the α-subunit and play critical roles in the regulation of sarcolemmal expression and gating of the Na^+ channel [35]. This highlights the benefit of studying the electrophysiological properties of ion channels using in vitro models that generate bona fide cardiomyocytes, rather than using heterologous expression systems that lack the correct cellular context of a cardiomyocyte.

Although there was no apparent difference in cardiac differentiation efficiency between the mESC and miPSC lines, it appears that the miPSC-CMs were more mature electrophysiologically than the corresponding mESC-CMs based on a larger I_{Na} density, more negative RMP, and higher V_{max} in the miPSC-CMs. The differences in peak I_{Na} density between the mESC- and miPSC-CMs was also present at day 10, and maintaining the mESC-CMs for >17 days in culture did not result in further increases in the I_{Na} density (Supplemental Figure 4). Additionally, the capacitance of the cardiomyocytes derived from all the mPSC lines was very similar, excluding the possibility that the functional differences were related to cell size. Therefore, we believe that these differences are most likely due to the inherent variability among ESC and iPSC lines to differentiate into cardiac cell types [36]. Indeed, others have also observed similar discrepancies [23].

Because the electrophysiological phenotype of the *Scn5a*-1798insD mutation was evident in both mESC- and miPSC-CMs, we wished to determine whether hiPSC-CMs bearing the *SCN5A*-1795insD mutation could also recapitulate the mixed biophysical properties of the disorder. We found a significant difference between control and SCN5A-het hiPSC-CMs in I_{Na} density, persistent I_{Na}, V_{max}, and APD_{90}, reflecting the loss- and gain-of-function phenotype of this Na^+ channel mutation and mirroring the findings in the mPSC models.

The V_{max} of our control hiPSC-CMs (115 V/s) was markedly higher than that reported by others (≈8–10 V/s) [18,19], partly because of our more negative RMP (−72.4 compared with −63.5 and −57.1 mV) and possible higher Na^+ channel expression. The RMP plays a critical role in Na^+ channel availability, which in turn determines upstroke velocity [37]. Any small changes in RMP will have a large effect on Na^+ channel inactivation, with the majority of channels in their inactivated state at more positive RMP. As a consequence, modeling Na^+ channel loss-of-function diseases such as BrS will be difficult in hiPSC-CMs that lack a rapid upstroke. The reason for the more negative RMP observed in our hiPSC-CMs is unclear but could possibly be due to the different differentiation method used (coculture with END-2 cells instead of EB differentiation), the inherent variability between PSC lines, and the fact that quiescent rather than spontaneously beating cardiomyocytes were selected for AP recordings.

It has been proposed that the *SCN5A*-1795insD mutation can cause both LQT3 and BrS, depending on the existing heart rate [38]. Indeed, in cardiomyocytes isolated from Scn5a-het mice, a prolonged APD occurs predominantly at slower pacing frequencies, whereas a decreased upstroke velocity is observed at higher rates [7]. Although the mixed phenotype was

present at all frequencies in the cardiomyocytes derived from the mPSCs, we did not observe the above features. This is possibly due to the limited APD_{90}-frequency relationship in mPSC models between 1 and 6 Hz, preventing more severe prolongation of the AP occurring at lower frequencies. In addition, because the APD_{90} in mPSC-CMs is shorter than in primary cardiomyocytes, the Na^+ channels might have sufficient time to recover from inactivation, thereby preventing a more pronounced reduction in V_{max} occurring at high frequencies. However, in SCN5A-het hiPSC-CMs, we observed a tendency toward a longer APD when the cells were paced at slower rates. Similarly, at faster rates, the relative reduction in V_{max} appeared larger in the SCN5A-het cardiomyocytes with respect to the corresponding wild-type cells. The ability to detect these differences in hiPSC-CMs might be due to their longer APD compared with the mouse models. Consequently, the time available for recovery from inactivation in the SCN5A-het hiPSC-CMs is shortened, potentially resulting in further reduction in Na^+ channel availability [8].

Conclusions

We have shown that multiple PSC models can recapitulate the diverse features of a *SCN5A* mutation with electrophysiological characteristics that are conserved in mice and humans. Our findings establish that both mouse and human PSCs can model a cardiac Na^+ channel overlap syndrome that evokes multiple cardiac rhythm disturbances. We also prove that miPSCs and hiPSCs can model loss-of-function Na^+ channel mutations, which, to the best of our knowledge, has not yet been shown. These findings extend and complement a recent publication demonstrating the ability of miPSCs to model a Na^+ gain-of-function mutation with altered gating properties [32] and suggest that hiPSCs might be able to emulate the electrophysiological aspects of other *SCN5A* mutations. Such models could prove beneficial for testing and developing novel pharmacological treatments for LQT3 and BrS patients. Overall, this study supports the notion that PSCs can be used to model inherited forms of cardiac disease and offers additional lines to the rapidly expanding list of cardiac disease iPSC models available.

Acknowledgments

We thank D. de Jong, K. Szuhai, and H. Tanke (Molecular Cell Biology, Leiden University Medical Center [LUMC]) for karyotyping analysis; S. Maas (Anatomy and Embryology, LUMC) for assistance with the teratoma analysis; and S. van de Pas (iPSC core facility, LUMC) for cell culture. We also thank S. Commandeur, A. el Ghalbzouri (Dermatology, LUMC), B.A. Schoonderwoerd, and M.P. van den Berg (Cardiology, Thoraxcenter, University Hospital Groningen) for control and *SCN5A* patient skin samples, as well as D. Atsma (Cardiology, LUMC) for obtaining approval from the Medical Ethics Committee. We are grateful to S. Braam and M. Bellin (Anatomy and Embryology, LUMC) for commenting on the manuscript.

Sources of Funding

This work was supported by the Netherlands Heart Foundation (Dr. Mummery, 2008B106; Dr. Bezzina, 2005T024), ZonMW (Drs. Mummery and Casini, 114000101), EU FP7 ("Industem"; Dr. Mummery, PIAP-GA-2008–230675), the Netherlands Institute of Regenerative Medicine (Dr. Mummery, C.W. van den Berg), the Netherlands Proteomics Consortium (Drs. Mummery, Freund, and Davis, 050-040-250), and the Interuniversity Cardiology Institute of the Netherlands (Dr. Remme, 061.02).

Disclosures

None.

Clinical Perspective

Clinical cardiology could benefit from greater insights into the pathology of cardiomyocytes in inherited cardiac disease. However, the availability of diseased cardiomyocytes is limited by the scarcity of biopsies from patients and the amount of tissue they yield. The advent of induced pluripotent stem cells, through which somatic cells can be genetically reprogrammed into stem cells able to differentiate to cardiomyocytes, now presents opportunities for solving this. However, a remaining issue is the extent to which the phenotype in these cells actually resembles that of cardiomyocytes in the heart itself. Here, we used reprogramming to investigate a cardiac overlap syndrome caused by a mutation in *SCN5A*, the sodium channel gene. Patients with this mutation (1795insD) can display symptoms of both long-QT syndrome type 3 and Brugada syndrome. We first derived induced pluripotent stem cells from mice with the corresponding *SCN5A* mutation. The derivative cardiomyocytes had electrophysiological properties similar to primary cardiomyocytes from the same heterozygous mutant mouse and from the embryonic stem cells used to generate it. The mutation resulted in a reduced Na^+ current density (Brugada syndrome) and prolonged action potential (long-QT syndrome type 3), demonstrating that stem cell-derived cardiomyocytes could recapitulate the functional characteristics responsible for the observed multiple phenotypes. We then derived induced pluripotent stem cells from a patient with the $SCN5A^{1795insD/+}$ mutation. The cardiomyocytes derived from these cells showed changes in the Na^+ channel biophysical properties similar to those in the mouse cardiomyocytes, demonstrating that human induced pluripotent stem cells could also model the pathognomonic features of the overlap syndrome. This model offers new opportunities for identifying drug effectiveness and sensitivities of clinical relevance.

References

1 Remme C.A., Bezzina C.R. Sodium channel (dys)function and cardiac arrhythmias. *Cardiovascular Therapeutics* 28: 287-294 (2010).

2 Amin A.S., Asghari-Roodsari A., Tan H.L. Cardiac sodium channelopathies. *Pflügers Archiv. European Journal of Physiology* 460: 223-237 (2010).

3 Bennett P.B., Yazawa K., Makita N., George A.L., Jr. Molecular mechanism for an inherited cardiac arrhythmia. *Nature* 376: 683-685 (1995).

4 Remme C.A., Wilde A.A., Bezzina C.R. Cardiac sodium channel overlap syndromes: different faces of SCN5A mutations. *Trends in Cardiovascular Medicine* 18: 78-87 (2008).

5 Bezzina C., Veldkamp M.W., van Den Berg M.P., Postma A.V. et al. A single Na(+) channel mutation causing both long-QT and Brugada syndromes. *Circulation Research* 85: 1206-1213 (1999).

6 van den Berg M.P., Wilde A.A., Viersma T.J.W., Brouwer J. et al. Possible bradycardic mode of death and successful pacemaker treatment in a large family with features of long QT syndrome type 3 and Brugada syndrome. *Journal of Cardiovascular Electrophysiology* 12: 630-636 (2001).

7 Remme C.A., Verkerk A.O., Nuyens D., van Ginneken A.C. et al. Overlap syndrome of cardiac sodium channel disease in mice carrying the equivalent mutation of human SCN5A-1795insD. *Circulation* 114: 2584-2594 (2006).

8 Remme C.A., Scicluna B.P., Verkerk A.O., Amin A.S. et al. Genetically determined differences in sodium current characteristics modulate conduction disease severity in mice with cardiac sodium channelopathy. *Circulation Research* 104: 1283-1292 (2009).

9 Remme C.A., Baartscheer A., Verkerk A.O., Engelen M.A. et al. Genetic background determines magnitude of late sodium current, extent of intracellular Na+ and Ca 2+ dysregulation, and severity of cardiomyopathy in murine sodium channelopathy. *Heart Rhythm* 6: 1686 (2009).

10 Veldkamp M.W., Viswanathan P.C., Bezzina C., Baartscheer A. et al. Two distinct congenital arrhythmias evoked by a multidysfunctional Na(+) channel. *Circulation Research* 86: E91-97 (2000).

11 Braam S.R., Passier R., Mummery C.L. Cardiomyocytes from human pluripotent stem cells in regenerative medicine and drug discovery. *Trends in Pharmacological Sciences* 30: 536-545 (2009).

12 Davis R.P., van den Berg C.W., Casini S., Braam S.R., Mummery C.L. Pluripotent stem cell models of cardiac disease and their implication for drug discovery and development. *Trends in Molecular Medicine* 17: 475-484 (2011).

13 Mummery C.L., Ward-van Oostwaard D., Doevendans P., Spijker R. et al. Differentiation of human embryonic stem cells to cardiomyocytes: role of coculture with visceral endoderm-like cells. *Circulation* 107: 2733-2740 (2003).

14 Sartiani L., Bettiol E., Stillitano F., Mugelli A. et al. Developmental changes in cardiomyocytes differentiated from human embryonic stem cells: a molecular and electrophysiological approach. *Stem Cells* 25: 1136-1144 (2007).

15 Jonsson M.K., Duker G., Tropp C., Andersson B. et al. Quantified proarrhythmic potential of selected human embryonic stem cell-derived cardiomyocytes. *Stem Cell Research* 4: 189-200 (2010).

16 Peng S., Lacerda A.E., Kirsch G.E., Brown A.M., Bruening-Wright A. The action potential and comparative pharmacology of stem cell-derived human cardiomyocytes. *Journal of Pharmacological and Toxicological Methods* 61: 277-286 (2010).

17 Jonsson M.K., van Veen T.A., Goumans M.J., Vos M.A. et al. Improvement of cardiac efficacy and safety models in drug discovery by the use of stem cell-derived cardiomyocytes. *Expert Opinion on Drug Discovery* 4: 357-372 (2009).

18 Moretti A., Bellin M., Welling A., Jung C.B. et al. Patient-specific induced pluripotent stem-cell models for long-QT syndrome. *The New England Journal of Medicine* 363: 1397-1409 (2010).

19 Itzhaki I., Maizels L., Huber I., Zwi-Dantsis L. et al. Modelling the long QT syndrome with induced pluripotent stem cells. *Nature* 471: 225-229 (2011).

20 Ma J., Guo L., Fiene S.J., Anson B.D. et al. High purity human-induced pluripotent stem cell-derived cardiomyocytes: electrophysiological properties of action potentials and ionic currents. *American Journal of Physiology: Heart and Circulatory Physiology* 301: H2006-2017 (2011).

21 Maltsev V.A., Wobus A.M., Rohwedel J., Bader M., Hescheler J. Cardiomyocytes differentiated in vitro from embryonic stem cells developmentally express cardiac-specific genes and ionic currents. *Circulation Research* 75: 233-244 (1994).

22 Fijnvandraat A.C., van Ginneken A.C., de Boer P.A., Ruijter J.M. et al. Cardiomyocytes derived from embryonic stem cells resemble cardiomyocytes of the embryonic heart tube. *Cardiovascular Research* 58: 399-409 (2003).

23 Kuzmenkin A., Liang H., Xu G., Pfannkuche K. et al. Functional characterization of cardiomyocytes derived from murine induced pluripotent stem cells in vitro. *FASEB Journal* 23: 4168-4180 (2009).

24 Takahashi K., Okita K., Nakagawa M., Yamanaka S. Induction of pluripotent stem cells from fibroblast cultures. *Nature Protocols* 2: 3081-3089 (2007).

25 Warlich E., Kuehle J., Cantz T., Brugman M.H. et al. Lentiviral vector design and imaging approaches to visualize the early stages of cellular reprogramming. *Molecular Therapy* 19: 782-789 (2011).

26 Carey B.W., Markoulaki S., Hanna J., Saha K. et al. Reprogramming of murine and human somatic cells using a single polycistronic vector. *Proceedings of the National Academy of Sciences of the United States of America* 106: 157-162 (2009).

27 Mummery C.L., van der Heyden M.A., de Boer T.P., Passier R. et al. Cardiomyocytes from human and mouse embryonic stem cells. *Methods in Molecular Medicine* 140: 249-272 (2007).

28 Freund C., Ward-van Oostwaard D., Monshouwer-Kloots J., van den Brink S. et al. Insulin redirects differentiation from cardiogenic mesoderm and endoderm to neuroectoderm in differentiating human embryonic stem cells. *Stem Cells* 26: 724-733 (2008).

29 Freund C., Davis R.P., Gkatzis K., Ward-van Oostwaard D., Mummery C.L. The first reported generation of human induced pluripotent stem cells (iPS cells) and iPS cell-derived cardiomyocytes in the Netherlands. *Netherlands Heart Journal* 18: 51-54 (2010).

30 Davis R.P., Ng E.S., Costa M., Mossman A.K. et al. Targeting a GFP reporter gene to the MIXL1 locus of human embryonic stem cells identifies human primitive streak-like cells and enables isolation of primitive hematopoietic precursors. *Blood* 111: 1876-1884 (2008).

31 Slager H.G., Van Inzen W., Freund E., Van den Eijnden-Van Raaij A.J., Mummery C.L. Transforming growth factor-beta in the early mouse embryo: implications for the regulation of muscle formation and implantation. *Developmental Genetics* 14: 212-224 (1993).

32 Malan D., Friedrichs S., Fleischmann B.K., Sasse P. Cardiomyocytes obtained from induced pluripotent stem cells with long-QT syndrome 3 recapitulate typical disease-specific features in vitro. *Circulation Research* 109: 841-847 (2011).

33 Matsa E., Rajamohan D., Dick E., Young L. et al. Drug evaluation in cardiomyocytes derived from human induced pluripotent stem cells carrying a long QT syndrome type 2 mutation. *European Heart Journal* 32: 952-962 (2011).

34 Yazawa M., Hsueh B., Jia X., Pasca A.M. et al. Using induced pluripotent stem cells to investigate cardiac phenotypes in Timothy syndrome. *Nature* 471: 230-234 (2011).

35 Wilde A.A., Brugada R. Phenotypical manifestations of mutations in the genes encoding subunits of the cardiac sodium channel. *Circulation Research* 108: 884-897 (2011).

36 Kattman S.J., Witty A.D., Gagliardi M., Dubois N.C. et al. Stage-specific optimization of activin/nodal and BMP signaling promotes cardiac differentiation of mouse and human pluripotent stem cell lines. *Cell Stem Cell* 8: 228-240 (2011).

37 Satin J., Kehat I., Caspi O., Huber I. et al. Mechanism of spontaneous excitability in human embryonic stem cell derived cardiomyocytes. *Journal of Physiology* 559: 479-496 (2004).

38 Clancy C.E., Rudy Y. Na(+) channel mutation that causes both Brugada and long-QT syndrome phenotypes: a simulation study of mechanism. *Circulation* 105: 1208-1213 (2002).

Supplemental Methods

Ethics Statement

All animal work was performed in accordance with institutional guidelines and national regulations. Human skin biopsies were obtained after individual permission using standard informed consent procedures and approval of the medical ethics committee of the Leiden University Medical Center and the Academic Medical Center, University of Amsterdam.

Generation of mouse induced pluripotent stem cells (miPSCs)

Primary mouse embryonic fibroblast (MEF) and adult tail-tip fibroblast (TTF) cells were obtained by mating *Scn5a*$^{1798insD/+}$ (Scn5a-het) and *Scn5a*$^{+/+}$ (Scn5a-wt) 129P2 mice. For TTF preparations, the postnatal mice were initially genotyped using material obtained from ear punch biopsies. Tails were then removed from Scn5a-wt and -het littermates, minced into pieces smaller than 1 mm, and cultured in MEF medium (DMEM supplemented with 2 mM L-glutamine, 10 mM non-essential amino acids (NEAA), 25 U/mL penicillin, 25 µg/mL streptomycin (all from Invitrogen), and 10 % FCS (Sigma)) until the fibroblast population emerged. To obtain MEFs, the embryos were harvested at embryonic day 13.5, and individual embryos dissected, digested with trypsin and cultured in MEF medium as described previously [1]. The heads of each embryo were used for genotyping. For miPSC generation, either TTFs or MEFs from littermates with the desired genotype were cultured in MEF medium for three passages or less and seeded one day before retroviral transduction at a density of 1 x 10^5 cells per well in a 6-well plate.

Retroviruses were produced in Plat-E cells that were cultured in MEF medium without antibiotics and independently transfected with one of the pMXs-based retroviral vectors encoding the mouse cDNA for *Oct4*, *Sox2*, *Klf4*, and *c-Myc* (Addgene plasmids 13366, 13367, 13370, and 13375) [2] by calcium phosphate-mediated transfection. Viral supernatants were harvested 48 h after transfection, combined, filtered through a 0.45 µm filter and used to infect the seeded fibroblasts in the presence of 8 µg/mL polybrene. The fibroblasts were incubated with fresh virus-containing supernatant 4, 8 and 24 h after the initial infection. The medium was replaced with fresh MEF medium 32 h after the final transduction. 48 h after the first transduction, the infected cells were harvested using trypsin and seeded between 1–3 x 10^4 cells/10 cm dish on mitotically-inactive MEF cells in mouse embryonic stem cell (mESC) culture medium. The cells were additionally treated with 1 mM valproic acid (Sigma) from 72 h post-infection for a total of 7 days. miPSC colonies morphologically resembling mESCs were picked approximately 14 days post-infection, dissociated with trypsin and subsequently expanded.

To ensure the resulting miPSC lines were clonal, dissociated miPSCs were labelled with an antibody for α-mouse SSEA-1 (Santa Cruz, sc-21702). The primary antibody was detected

with FITC-conjugated goat α-mouse IgM (Jackson Immuno Research). Using the single-cell deposition function of a FACSaria FACS station, single SSEA-1^{+} miPSCs were placed into wells of 96-well plates preseeded with mitotically-inactive MEF cells and containing mESC culture medium. Clonal Scn5a-wt and-het miPSC colonies were visible 7 days after sorting. One miPSC clone for each genotype was subsequently selected, dissociated with trypsin and expanded for use in this study. The genotype of the *Scn5a*$^{+/+}$ and *Scn5a*$^{1798ins/+}$ miPSCs was re-confirmed.

Generation of human iPSCs

Dermal fibroblasts from a 47 year-old male patient with the *SCN5A*-1795insD mutation and from a 51 year-old unaffected female were isolated from skin biopsies. The samples were incubated in 25 U/mL dispase/PBS (both from Invitrogen) overnight at 4 °C before removing the epidermal tissue and mincing the remaining material into <1 mm pieces. This was further dissociated for 2 h at 37 °C using a solution containing 0.75 % collagenase A (Roche) and 2 U/mL dispase, before plating on tissue culture dishes in Fibroblast Medium (DMEM supplemented with 2 mM L-glutamine, 10 mM NEAA, 25 U/mL penicillin, 25 µg/mL streptomycin, 1 mM sodium pyruvate (Invitrogen), 10 µg/mL ascorbic acid and 10 % FCS (both Sigma)). Fibroblasts appeared within 3 days and were transduced with the lentiviruses within 4 passages.

Lentiviruses containing an inducible or self-inactivating multicistronic cassette encoding OCT3/4, SOX2, KLF4, and c-MYC [3,4] (Addgene plasmid 20321; "4-in-1" SIN reprogramming vector kindly provided by C. Baum) were produced in the HEK293T cell line, cultured in Fibroblast Medium. The cells underwent calcium phosphate- or polyethylenemine-mediated co-transfection of the expression plasmid with pCMV-VSVG (encoding the vesicular stomatitis virus glycoprotein), pMDLg-RRE (encoding HIV-1 gag/pol), and pRSV-REV (encoding HIV-1 rev). Supernatants containing the lentiviral particles were harvested 48 h after transfection and filtered through a 0.45 µm filter.

One day prior to lentiviral infection, 1.25 x 10^5 fibroblasts were plated in Fibroblast Medium in a well of a 6-well plate. The cells were incubated with either the inducible or self-inactivating lentivirus for 12 h in the presence of 4 µg/mL polybrene. Two days after transduction, the cells were harvested and seeded on MEFs at a density of 4 x 10^4 cells/10 cm dish and cultured in hESC KOSR Medium (Dulbecco's Modified Eagle Media (DMEM)/F12 supplemented with Glutamax, 10 mM NEAA, 25 U/mL penicillin, 25 µg/mL streptomycin, 100 µM β-mercaptoethanol, 20 % knockout serum replacement (KOSR; Invitrogen) and 10 ng/mL basic FGF (PreproTech)). Medium was changed daily. For reprogramming with the inducible lentivirus, the hESC KOSR Medium was supplemented with 1 µg/mL doxycycline (Sigma Aldrich) for the first 10 days, and then reduced to 0.5 µg/mL for another 2 days. HESC-like colonies were picked approximately 5 weeks after transduction, and subsequently cultured and expanded in mTeSR1 according to the manufacturer's protocol (Stem Cell Technologies).

Culture and differentiation of mouse pluripotent stem cells (PSCs)

Mouse ESCs and iPSCs were maintained on irradiated MEFs in mESC culture medium consisting of DMEM supplemented with 15 % FCS, 0.1 mM β-mercaptoethanol, 2 mM L-glutamine, 10 mM NEAA, 25 U/mL penicillin, 25 µg/mL streptomycin, 1:100 nucleosides and 10^3 U/mL mouse leukemia inhibitory factor (both from Millipore). Every 2 to 3 days the mPSCs were passaged as previously described for mESCs [1].

Before inducing differentiation, mESCs and miPSCs were passaged minimally three times on 0.1 % gelatin-coated tissue culture dishes in mESC culture medium supplemented with 4 mM CHIR 99021 and 1 mM PD0325901 (both from Axon Medchem) to eliminate MEFs. Mouse PSCs were differentiated as embryoid bodies (EBs) using a "hanging drop" protocol [1] in mESC differentiation medium (Iscove's Modified Dulbecco's Medium supplemented with 5 % protein-free hybridoma media II (both from Invitrogen), 15 % FCS (Greiner), 2 mM L-glutamine, 50 mg/mL ascorbic acid, 25 U/mL penicillin, 25 µg/mL streptomycin and 450 µM monothioglycerol (Sigma Aldrich)). For spontaneous differentiation, day 7 EBs were plated on gelatin-coated glass coverslips and analysed at day 17 of differentiation for expression of markers of the three germ layers.

For differentiation towards the cardiac lineages, unless stated otherwise, the EBs were transferred to non-adherent culture dishes (Nunc) at day 5 of differentiation and the mESC differentiation medium supplemented with 10^{-8} M all-*trans* retinoic acid (RA, Sigma Aldrich) for 9 days. On day 7 of differentiation, these EBs were seeded on gelatin-coated tissue-culture dishes. EBs were collected for RNA isolation at time points indicated in the figure. To reduce the proliferation of non-cardiomyocytes, the concentration of FCS was reduced to 5 % on day 14 of differentiation. Beating areas from differentiated EBs were microscopically dissected and dissociated using TrypLE Select (Invitrogen). The dissociated cells were seeded on gelatin-coated glass coverslips in 5 % FCS-containing mESC differentiation medium for electrophysiological and immunofluorescence analysis.

Culture and differentiation of human iPSCs

Human iPSCs were cultured as previously reported for hESCs [5] either on mitomycin C-treated MEFs in hESC Medium or on Matrigel-coated tissue culture dishes in mTeSR1 according to the manufacturer's protocol (Stem Cell Technologies). Human iPSCs were induced to differentiate to cardiomyocytes by co-culture on visceral endoderm-like (END-2) cells as described previously [5,6]. For differentiation of hiPSCs from mTeSR1-maintained cultures, colonies were enzymatically dissociated into small clumps using dispase (Invitrogen) and cultured overnight in ultralow attachment plates (Costar) in hESC Medium supplemented with 5 µM fasudil monohydrochloride (LC Laboratories). The resulting EBs were subsequently transferred to co-cultures with END-2 cells, or cultured in suspension for 8 days in hESC Medium before plating on gelatin-coated coverslips in the same medium. Analysis for expression of markers of the

three germ layers was performed on EBs at day 16 of differentiation. For electrophysiological and immunofluorescence analysis of cardiomyocytes, beating aggregates following 15–18 days of co-culture were dissociated into single cells using collagenase [1] and replated on gelatin-coated coverslips in DMEM containing 20 % FCS. Twenty-four hours after plating, the amount of FCS in the medium was decreased to 5 %.

Teratoma formation and analysis

Undifferentiated mouse iPSCs were dissociated into single cells and between 5 x 10^4 and 4 x 10^5 cells were injected into the testis of NOD/SCID mice. Teratomas were collected 4–9 weeks after injection, fixed with 10 % buffered formalin and embedded in paraffin. The samples were processed by 5 µm cryo-sectioning, stained with haematoxylin and eosin, and analysed under light microscopy.

Genomic DNA isolation and genotyping the *Scn5a* locus

Genomic DNA was isolated from the tissue biopsies and cultured cells using a phenol/chloroform extraction procedure as described previously [7]. The genotype of the *Scn5a*$^{+/+}$ and *Scn5a*$^{1798insD/+}$ mice, fibroblasts, mESCs and miPSCs was determined using a PCR-digest as described previously [8]. Briefly, a region of the 3' UTR of the *Scn5a* locus was amplified from genomic DNA using forward (5'-CTCCAGCTCTTCCATCTCCTCC-3') and reverse (5'-GCTACTAGGGTGTGCCAGGCC-3') primers under standard PCR conditions (30 cycles of 94 °C, 20 seconds; 60 °C, 30 seconds; 68 °C, 40 seconds). The resulting 378 bp PCR product was digested with *EcoR*V (Promega) at 37 °C for 2 hours, and visualised following agarose gel electrophoresis. Because the *Scn5a*^{1798insD} allele contains a silent *EcoR*V site, *EcoR*V digestion of the PCR product from this allele results in 202 bp and 188 bp DNA fragments, while the PCR product generated from the wild-type allele remains 388 bp.

To confirm the presence or absence of the *SCN5A*-1795insD mutation in the hiPSCs, the relevant region of the *SCN5A* locus was amplified from genomic DNA using forward (5'-AAGTGGGAGGCTGGCATCGAC-3') and reverse (5'- CCGCCTGCTGACGGAAGAGGA-3') primers under standard PCR conditions (32 cycles of 94 °C, 30 seconds; 60 °C, 30 seconds; 68 °C, 60 seconds). The PCR products were purified using the QIAquick PCR Purification kit (Qiagen) and sequenced using the forward primer.

Karyotype analysis

Karyotype analysis was performed using COBRA-FISH as described elsewhere [9]. 20 metaphase spreads for each sample were analysed.

Immunofluorescence analysis

EBs and single cells were fixed in 2 % paraformaldehyde, permeabilised with phosphate buffered saline (PBS)/0.1 % Triton-X 100 (Sigma-Aldrich) and blocked with PBS/4 % swine serum (Dako). Samples were incubated overnight at 4 °C with primary antibodies, and the primary antibodies detected by incubating with either Alexa Fluor 488- or 532-, Cy3- or FITC-conjugated secondary antibodies at room temperature for 1 hour. The primary antibodies and corresponding secondary antibodies are listed in Supplemental Table 1. Nuclei were stained with 4', 6-Diamidino-2-Phenylindole (DAPI, Invitrogen). Images were captured using a Leica SP5 confocal laser scanning microscope (Leica Microsystems).

Gene-expression analysis

Total RNA was purified using the RNeasy Mini Kit (Qiagen) according to the manufacturer's protocol. RNA samples were reverse transcribed using the SuperScript II First-Strand Synthesis kit (Invitrogen). PCR gene expression analysis was performed under standard conditions (25–35 cycles of 94 °C, 20 seconds; 60 °C, 30 seconds; 68 °C, 60 seconds) using the primer sets listed in Supplemental Table 2.

Electrophysiology

Data Acquisition and Analysis

Electrophysiological recordings were performed on single cardiomyocytes (CMs), identified on the basis of their typical morphology, 2–3 days after cell dissociation for mPSC-CMs and 8–10 days for hiPSC-CMs. For human iPSC-CMs this time range was chosen, as it was optimal for the development of I_{Na} in human ESC-CMs (S. Casini, C.L. Mummery, unpublished findings). Data were collected from a minimum of 4 independent differentiations per line. For action potential (AP) measurements, quiescent cardiomyocytes that contracted upon field stimulation were selected. I_{Na} and APs were measured respectively with the ruptured or perforated patch-clamp technique using an Axopatch 200B amplifier (Molecular Devices). Voltage control, data acquisition, and analysis of I_{Na} and APs were performed with pClamp10.0/Clampfit (Axon Instruments) and custom-made software, respectively. Adequate voltage control was achieved with low-resistance pipettes (1.5–2.5 MΩ), series resistance (Rs) and cell membrane capacitance (Cm) compensation ≥80 %, and by maintaining a fraction of channels in their inactivated state by using a holding potential of –90 mV. I_{Na} and APs were filtered at 5 kHz and digitized at 20 and 40 kHz, respectively. Potentials were corrected for the estimated change in liquid junction potential (15 mV), except for I_{Na} measurements, where it was 5 mV.

I_{Na} measurements

I_{Na} and persistent I_{Na} recordings were performed using an extracellular solution containing (in mM): 130 NaCl, 10 CsCl, 1.8 $CaCl_2$, 1.2 $MgCl_2$, 11.0 glucose, 5.0 HEPES, and 5 µM nifedipine;

pH 7.3 (CsOH). The pipette solution contained (in mM): 3.0 NaCl, 133 CsCl, 2.0 $MgCl_2$, 2.0 Na_2ATP, 2.0 TEACl, 10 EGTA, 5.0 HEPES; pH 7.2 (CsOH). I_{Na} densities and gating properties were measured at room temperature using voltage-clamp protocols shown in the relevant figures. Measurements were performed using a holding potential of −90 mV with a cycle time of 5 seconds, except for recovery of inactivation and development of slow inactivation where a cycle time of 8 seconds was used. Persistent I_{Na} was measured as a TTX-sensitive current at 36±0.2 °C either using a descending ramp protocol, or a 200 ms depolarizing step to −30 mV from a holding potential of −90 mV. Current densities were calculated by dividing current amplitude by Cm. Cm was determined by dividing the decay time constant of the capacitive transient in response to 5 mV hyperpolarizing steps from −40 mV, by the Rs.

Voltage-dependence of activation and inactivation curves were fitted with a Boltzmann function ($y=[1+\exp\{(V-V_{1/2})/k\}]^{-1}$), where $V_{1/2}$ is the half-maximal voltage of (in)activation and k is the slope factor. Recovery from inactivation was assessed with a double pulse protocol. Data were normalised to the current elicited by the first pulse (P1) and fitted with a bi-exponential function ($y=y_0+A_f\{1-\exp[-t/\tau_f]\}+A_s\{1-\exp[-t/\tau_s]\}$), where A_f and A_s represent the amplitudes of the fast and the slow components of recovery from inactivation, and τ_f and τ_s are their respective recovery time constants. Development of slow inactivation was fitted with a single exponential function ($y=A+A_0\exp[t/\tau]$) where τ is the time constant for the development of slow inactivation and A is the fraction of channels that enter the slow inactivated state after a 3000 ms depolarising step.

AP measurements

APs were measured at 36±0.2 °C using a modified Tyrode's solution containing (in mM): 140 NaCl, 5.4 KCl, 1.8 $CaCl_2$, 1.0 $MgCl_2$, 5.5 glucose, 5.0 HEPES; pH 7.4 (NaOH). The pipette solution contained (in mM): 125 K-gluconate, 20 KCl, 10 NaCl, 0.22 amphotericin-B, 10 HEPES; pH 7.2 (KOH). APs were elicited at 1, 3, or 6 Hz in mPSC-CMs and at 1, 2, or 3 Hz in hiPSC-CMs by 3 ms, 1.2x threshold current pulses through the patch pipette. The resting membrane potential (RMP), maximal upstroke velocity (V_{max}), AP amplitude (APA), and AP duration (APD) at 20, 50 and 90 % repolarisation (APD_{20}, APD_{50}, and APD_{90}, respectively) were analysed. Data from 10 consecutive APs were averaged.

Supplemental Table 1. Antibodies used for immunofluorescence analysis

Antibody	Supplier	Dilution
Mouse-α-rabbit α-Actinin (sarcomeric)	Sigma Aldrich; A7811	1:800
Mouse-α-human α-SMA Clone 1A4	Sigma Aldrich; A2547	1:500
Mouse-α-human β-MHC	Millipore; MAB1548	1:50
Rabbit-α-bovine GFAP	DAKO; Z0334	1:100
Rabbit-α-mouse MLC2a	Provided by S.W. Kubalak	1:2000
Rabbit-α-mouse Nanog	Abcam; ab80892	1:100
Goat-α-human NANOG	R&D Systems; AF1997	1:20
Goat-α-human Oct3/4	Santa Cruz; SC-8628	1:100
Rabbit-α-rat Scn5a	Alomone Labs; ASC-005	1:300
Goat-α-human SOX17	R&D systems; MAB1924	1:100
Mouse-α-mouse SSEA-1	Santa Cruz; SC-21702	1:100
Mouse-α-human SSEA4	Santa Cruz; sc-59368	1:100
Mouse-α-human TRA-1-81	Millipore; MAB4381	1:100
Rabbit-α-human TROPONIN I	Santa Cruz; sc-15368	1:500
FITC-conjugated goat-α-mouse IgM	Jackson ImmunoResearch; 115-095-075	1:100
Alexa Fluor 488-cojugated donkey-α-rabbit IgG	Invitrogen; A21206	1:100
Alexa Fluor 532-cojugated goat-α-mouse IgG	Invitrogen; A11002	1:100
Cy3-conjugated donkey-α-goat IgG	Jackson ImmunoResearch; 705-165-147	1:100
Cy3-conjugated goat-α-mouse IgG	Jackson ImmunoResearch; 115-165-146	1:250
Cy3-conjugated goat-α-mouse IgM	Jackson ImmunoResearch; 115-165-020	1:100
Cy3-conjugated donkey-α-mouse IgG	Jackson ImmunoResearch; 715-165-150	1:200
Cy3-conjugated donkey-α-rabbit IgG	Jackson ImmunoResearch; 711-165-152	1:100

FITC, Fluorescein isothiocyanate; Cy3, Cyanine3

Supplemental Table 2. Primers used for RT-PCR analysis of endogenous genes with corresponding PCR product sizes

Genes	Sense primer	Antisense primer	Size (bp)
Oct4	5'-CCAACGAGAAGAGTATGAGGCTA-3'	5'-CAAAATGATGAGTGACAGACAGG-3'	392
Nanog	5'-ATGGTCTGATTCAGAAGGGCTC-3'	5'-CTGCAACTGTACGTAAGGCTG-3'	299
Sox2	5'-TAGAGCTAGACTCCGGGCGATGA-3'	5'-TTGCCTTAAACAAGACCACGAAA-3'	297
Rex1	5'-GATTCACATCCTAACCCACGCA-3'	5'-GCTTTCACCATTCACTTTCCTG-3'	239
Ecat	5'-CGGCTTCGGTGCAGGTTCGTG-3'	5'-CTGCCTTTAGGTTCTGGATTTGC-3'	380
Gapdh	5'-GTTTGTGATGGGTGTGAACCAC-3'	5'-CTGGTCCTCAGTGTAGCCCAA-3'	451
Brachyury	5'-CTGTGGCTGCGCTTCAAGGA-3'	5'-GTGGATGTAGACGCAGCTGG-3'	228
Mixl1	5'-CGAGTCCAGGATCCAGGTGTG-3'	5'-GAGCCAATATCTTCAGAGAGAGAC-3'	267
Mesp1	5'-CATCGTTCCAGTACGCAGAAAC-3'	5'-GCTCAGACAGGGTGACAATCATC-3'	183
Nkx2.5	5'-CAAGTGCTCTCCTGCTTTCC-3'	5'-GGCTTTGTCCAGCTCCACT-3'	136
Tbx5	5'-CTGTACCAAGAGGAAAGATGAGG-3'	5'-TCCAGGCTAGGCACGGGCTCGC-3'	216
Scn5a	5'-GCGGGCTGGCTGCTCCTACCTACC-3'	5'-CTCTCCAAGCCTCGAGAGCAAAGTA-3'	284
Mlc2v	5'-AAAGAGGCTCCAGGTCCAAT-3'	5'-CCTCTCTGCTTGTGTGGTCA-3'	177

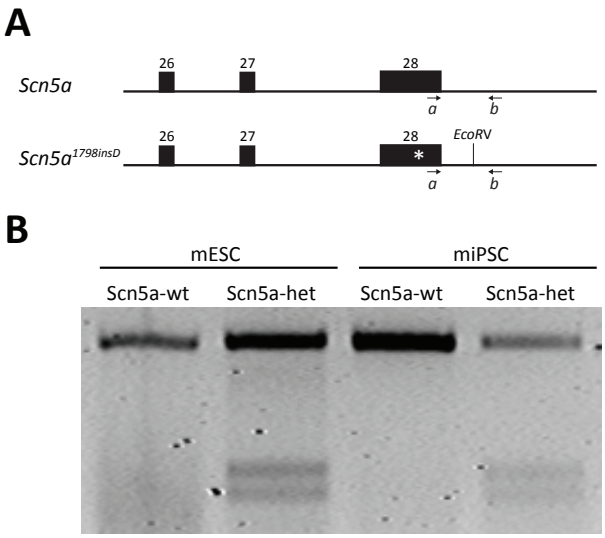

Supplemental Figure 1. Genotyping of control and Scn5a-het miPSC lines
A, Structure of the wild-type (*Scn5a*$^{+/+}$) and *Scn5a*^{1798insD} alleles in the Scn5a-het miPSCs. The * indicates the 1798insD mutation in exon 28 (black box). An *EcoR*V restriction site is located 3' of exon 28 in the *Scn5a*^{1798insD} allele, but is absent from the *Scn5a* allele. The position of primers (*a*,*b*) used to identify the genotype of the miPSCs are shown. **B**, PCR-digest genotyping (primers *a* & *b*, followed by *EcoR*V digestion) of genomic DNA from the mESCs and miPSCs confirmed the genotype of the Scn5a-wt and Scn5a-het mESC and miPSC clones. Digestion of the PCR product with *EcoR*V resulted in a 378 bp DNA fragment from the Scn5a-wt mPSCs. From Scn5a-het mPSCs, three bands following *EcoR*V digestion were obtained – a 378 bp DNA fragment from the *Scn5a*$^{+/+}$ allele, and 202 bp and 188 bp DNA fragments from the *Scn5a*^{1798insD} allele.

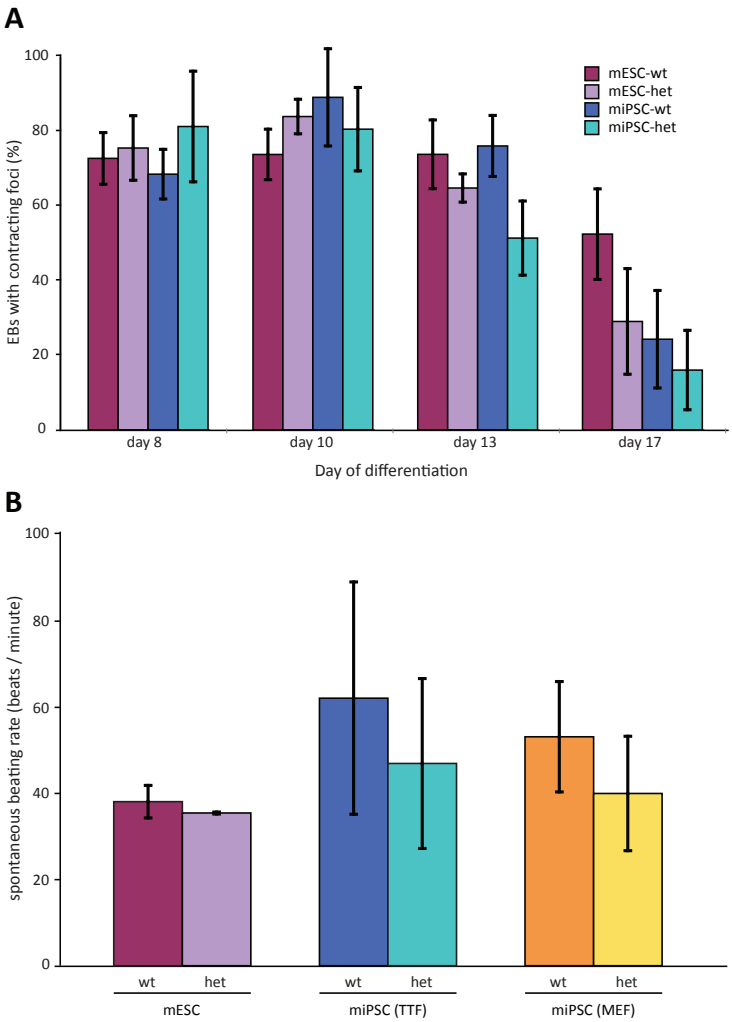

Supplemental Figure 2. Characterisation of Scn5a-wt and -het mPSC-CMs

A, Proportion of embryoid bodies (EBs) derived from Scn5a-wt and Scn5a-het mESCs and miPSCs containing spontaneously contracting foci. Scn5a-wt and Scn5a-het mPSCs underwent EB differentiation and the percentage of EBs containing spontaneously contracting foci was determined at various time points (n=3 separate differentiations). By day 8 of differentiation, between 69 % (Scn5a-wt miPSC) and 82 % (Scn5a-het miPSC) of the EBs contained spontaneously contracting regions. By day 10 of differentiation, these proportions had remained static or increased up to a maximum of 90 % (EBs from Scn5a-wt miPSCs). Subsequently (day 13 of differentiation), the proportion of EBs with contracting foci decreased, and by day 17 of differentiation between 16 % (Scn5a-het miPSC) and 53 % (Scn5a-wt mESC) of EBs contained microscopic contracting foci. **B**, Frequency of spontaneous contractions in mPSC-derived EBs at day 10 of differentiation. Scn5a-wt and -het EBs were formed from either the mESC lines or from the miPSC lines derived from tail tip fibroblasts (TTF) or embryonic fibroblasts (MEF), and the spontaneous beating rate determined from at least 28 different EBs per cell line (n=3 separate differentiations). Error bars represent the SEM. Statistical comparisons of samples were performed by either one-way ANOVA (A), or t-test (B). No significant differences were detected. wt, *Scn5a*$^{+/+}$; het, *Scn5a*$^{1798insD/+}$.

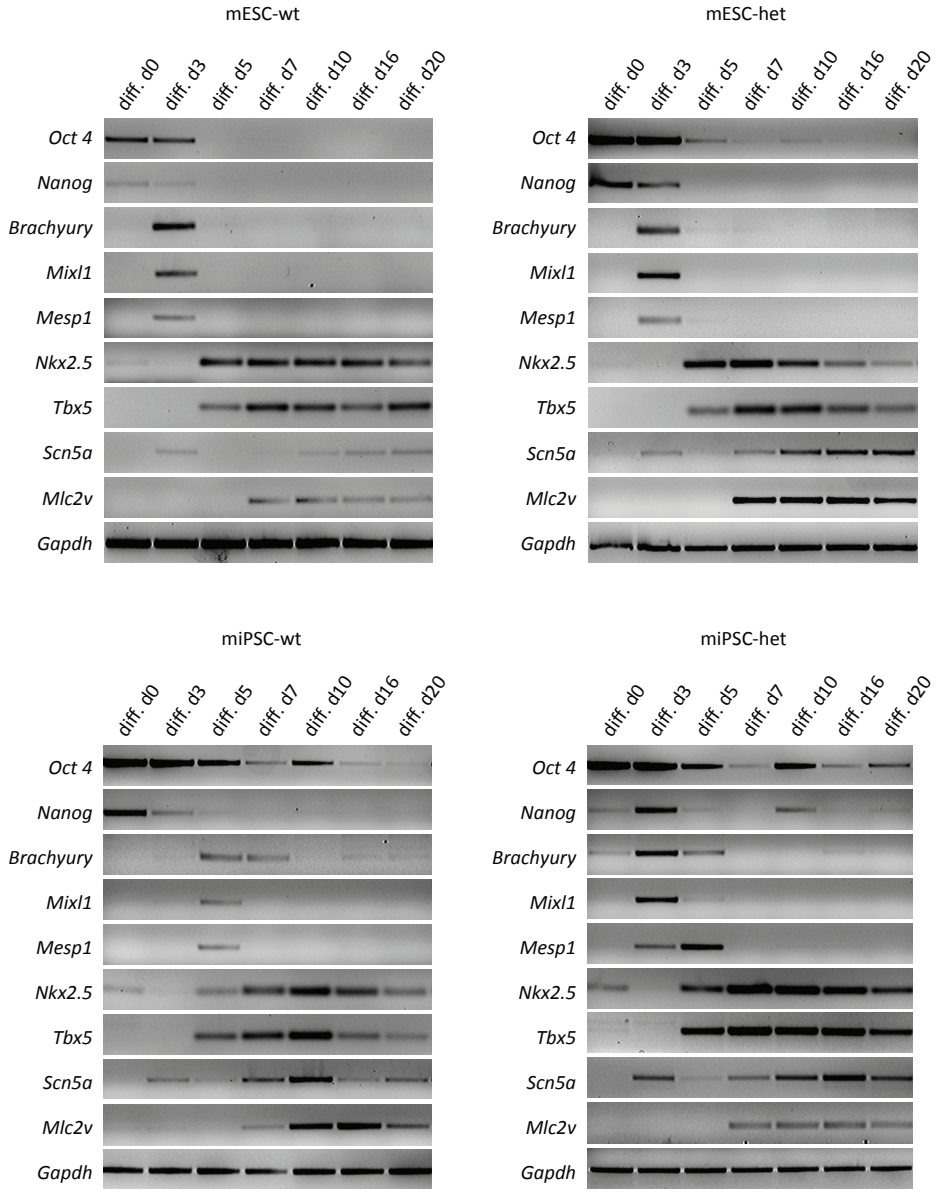

Supplemental Figure 3. Gene expression patterns of differentiating Scn5a-wt and Scn5a-het mESC and miPSCs

Differentiating Scn5a-wt and Scn5a-het miPSCs induced expression of pluripotency, primitive streak, cardiac mesoderm, and cardiac genes with an expression pattern comparable to differentiating Scn5a-wt and Scn5a-het mESCs. Total RNA was collected from the mPSC lines at the timepoints indicated (d, day). Semi-quantitative RT-PCR analysis showed the progressive down-regulation of the stem cell markers, *Oct4* and *Nanog*, the transient expression of the primitive streak genes, *Brachyury* and *Mixl1*, and the cardiac mesodermal marker, *Mesp1*, and the activation of genes expressed in cardiac cell types (*Nkx2.5*, *Tbx5*, *Scn5a* and *Mlc2v*). *Gapdh* was used as a loading control. wt, $Scn5a^{+/+}$; het, $Scn5a^{1798insD/+}$.

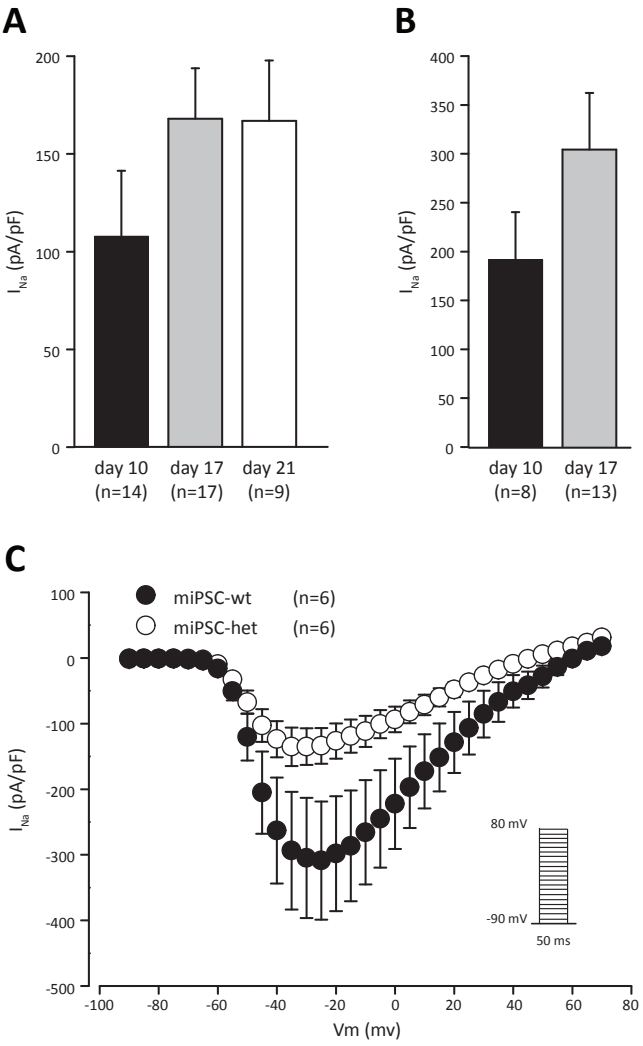

Supplemental Figure 4. Average I_{Na} densities in mESC- and miPSC-CMs
A, Average peak Na^+ current densities for Scn5a-wt mESC-CMs measured at day 10 (−107.8±33.6 pA/pF), day 17 (−168.1±24.2 pA/pF) and day 21 (−166.9±30.9 pA/pF). The Cm of the cells was 18.4±1.8 pF, 22.2±2.0 pF, and 18.2±2.1 pF, respectively. **B**, Average peak Na^+ current densities for Scn5a-wt miPSC-CMs measured at day 10 (−191.7±48.7 pA/pF) and day 17 after dissociation (−304.4±57.9 pA/pF). The Cm of the cells was 18.5±1.8 pF and 16.4±1.6 pF, respectively. Based on the results shown in A and B, we performed all further electrophysiological characterisation of the mPSC-CMs at day 17. **C**, Average Na+ current-voltage relationships for cardiomyocytes derived from Scn5a-wt and Scn5a-het miPSCs. These miPSC lines were generated from MEFs isolated from mice of the same litter. In Scn5a-het miPSC-CMs, I_{Na} density was decreased compared to the control cardiomyocytes. I_{Na} density values for Scn5a-wt miPSC-CMs (−304.8±91.7 pA/pF, at −30 mV) and Scn5a-het miPSC-CMs (−135.1±27.9 pA/pF, at −30 mV) were similar to those observed in cardiomyocytes differentiated from miPSC lines that had been derived from adult mouse tail-tip fibroblasts. Inset depicts voltage protocol. Statistical comparisons of samples were performed by one- way ANOVA (A), t-test (B), or two-way rmANOVA (C). No significant differences were detected. wt, *Scn5a*$^{+/+}$; het, *Scn5a*$^{1798insD/+}$.

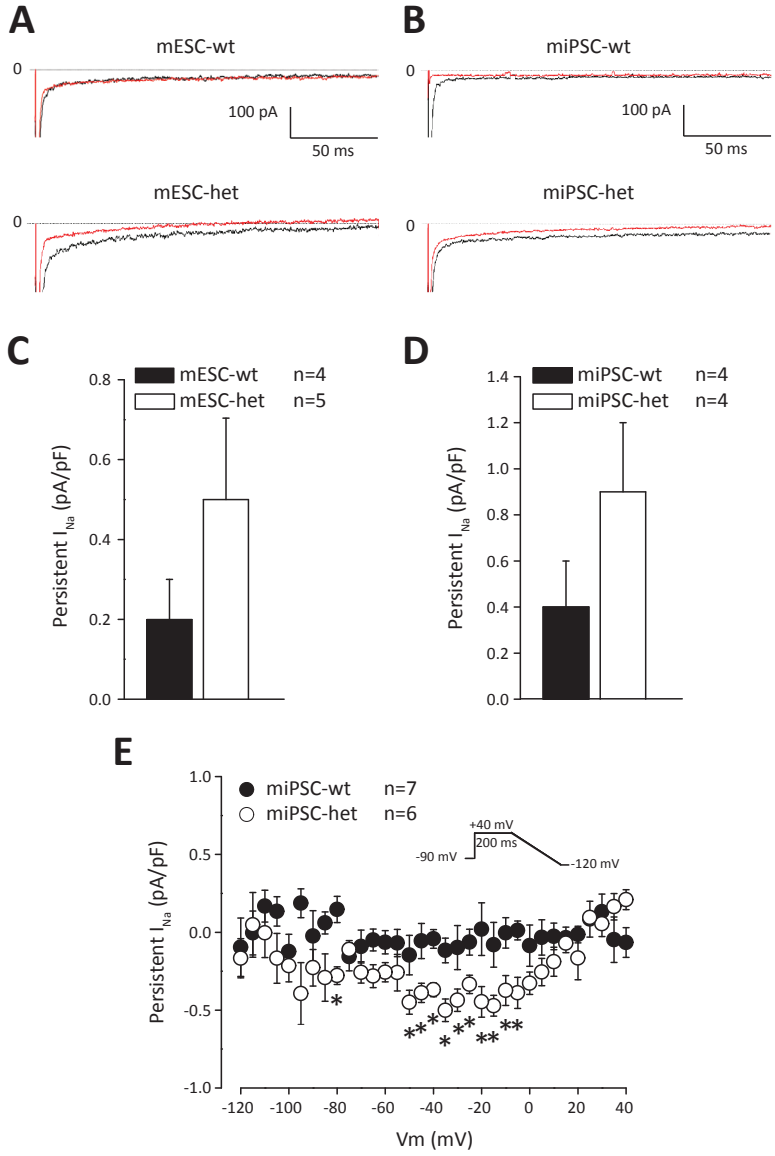

Supplemental Figure 5. Persistent I_{Na} measurements in Scn5a-wt and Scn5a-het mESC- and miPSC-CMs

A and **B**, Examples of persistent I_{Na} traces recorded at −30 mV in control conditions (black line) and after application of 30 µM TTX (red line) in Scn5a-wt (top) and Scn5a-het (bottom) cardiomyocytes derived from mESCs (A) and miPSCs (B). **C** and **D**, Average values for persistent I_{Na} densities at the end of the depolarising step, measured as the TTX-sensitive current, in mESC-CMs (Scn5a-wt: −0.2±0.1 pA/pF; Scn5a-het: −0.5±0.2 pA/pF; C) and miPSC-CMs (Scn5a-wt: −0.4±0.2 pA/pF; Scn5a-het: −0.9±0.3 pA/pF; D). **E**, Average values for persistent I_{Na} density in a second independent set of Scn5a-wt and-het miPSC-CMs. These miPSC lines were generated from MEFs isolated from mice of the same litter. Statistical comparisons of samples were performed by t-test (C and D), or two-way rmANOVA (E). * indicates statistical significance (P<0.05). Voltage protocol is shown as inset. wt, *Scn5a*$^{+/+}$; het, *Scn5a*$^{1798insD/+}$.

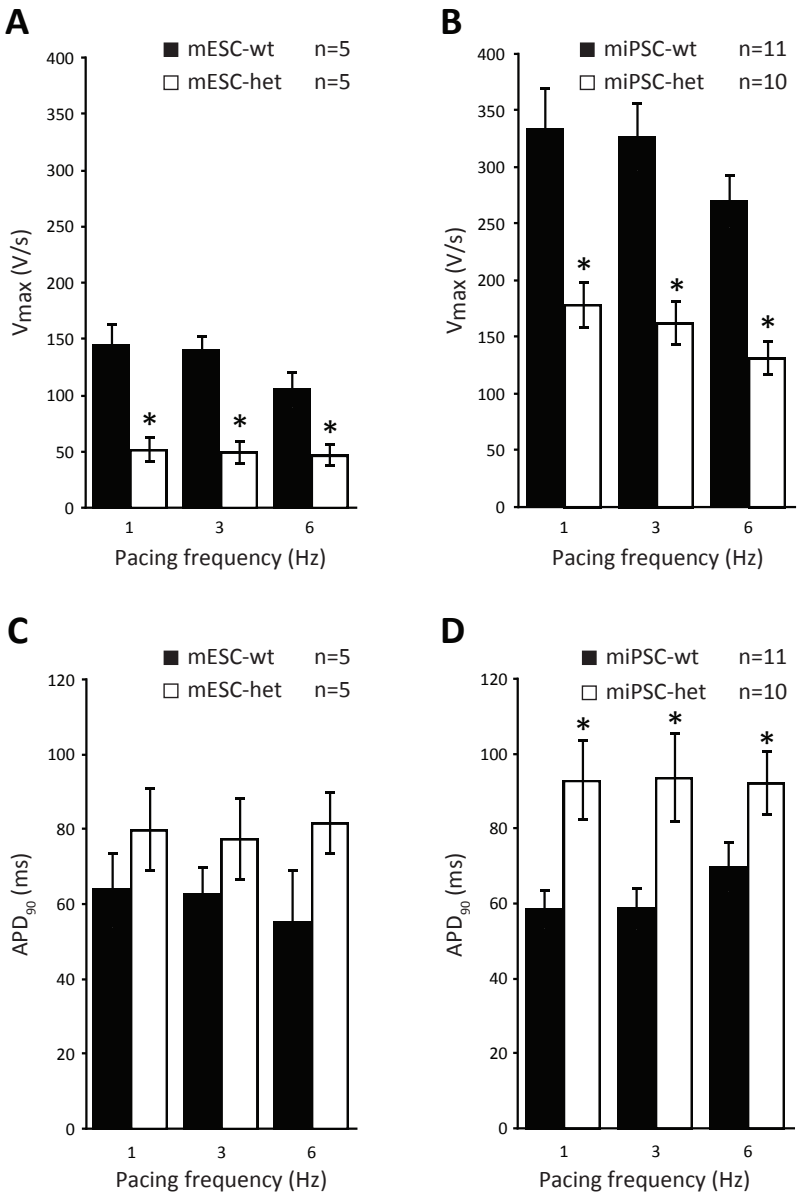

Supplemental Figure 6. Action potential (AP) properties in Scn5a-wt and -het mPSC- CMs
Average data at the stimulation frequencies of 1, 3 and 6 Hz for upstroke velocity (V_{max}) (**A**, **B**) and AP duration 90 % repolarisation (APD_{90}) (**C**, **D**) in Scn5a-wt and Scn5a-het cardiomyocytes derived from mESCs (A, C) and miPSCs (B, D). * indicates statistical significance (P<0.05; two-way rmANOVA). wt, *Scn5a*$^{+/+}$; het, *Scn5a*$^{1798insD/+}$.

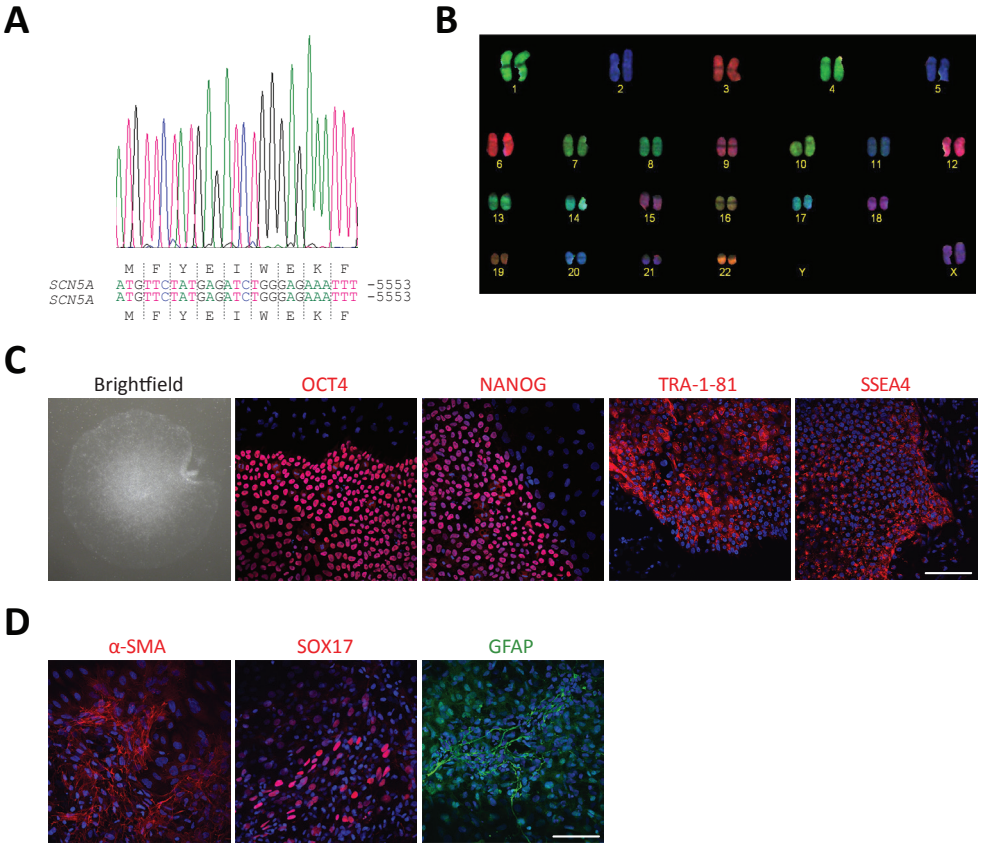

Supplemental Figure 7. Characterisation of SCN5A-wt hiPSCs

A, Sequence analysis of SCN5A-wt hiPSCs confirming both alleles are unmodified around position 5388 of the *SCN5A* locus. **B**, COBRA-FISH karyogram of SCN5A-wt hiPSCs showing a normal 46XX karyotype. **C**, Shown from left to right; a brightfield image (original magnification, x16) of; and immunofluorescent images for OCT3/4, NANOG, TRA-1-81 and SSEA4 in SCN5A-wt hiPSCs. Nuclei were stained with DAPI (blue). **D**, Immunostaining of embryoid bodies from SCN5A-wt hiPSCs for the differentiation markers α-smooth muscle actin (α-SMA), SOX17, and glial fibrillary acidic protein (GFAP). Nuclei were stained with DAPI. Scale bars in B and D represent 100 µm. wt, *SCN5A*$^{+/+}$.

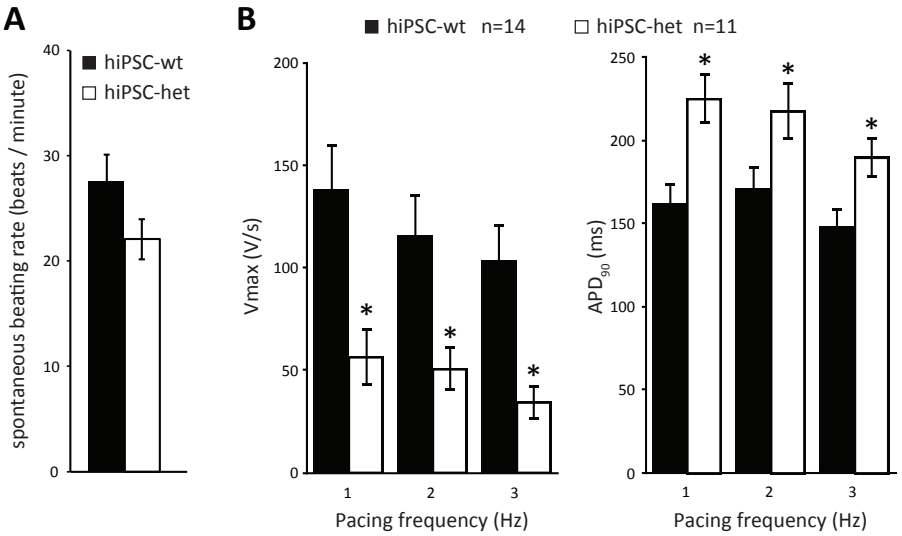

Supplemental Figure 8. Characterisation of SCN5A-wt and -het hiPSC-CMs
A, Rate of spontaneous contractions of SCN5A-wt and-het hiPSC-CMs at 12 days of differentiation. Data was averaged from at least 40 spontaneously beating areas (n=4 separate differentiations). Samples were compared by t-test with no significant difference detected. **B**, Average data for upstroke velocity (V_{max}) (left), and action potential duration at 90 % repolarisation (APD_{90}) (right) measured at 1, 2, 3 Hz for SCN5A-wt and-het hiPSC-CMs following 18 days of co-culture with END-2 cells. * indicates statistical significance (P<0.05; two-way rmANOVA). wt, *SCN5A*$^{+/+}$; het, *SCN5A*$^{1795insD/+}$.

Supplemental Movie 1
Movie of day 8 embryoid bodies derived from *Scn5a*-wt and Scn5a-het mESCs and miPSCs containing spontaneous contracting areas.

Supplemental Movie 2
Movie of *SCN5A*-wt and *SCN5A*-het hiPSCs at day 12 of differentiation containing spontaneously contracting areas.

Supplemental References

1 Mummery C.L., van der Heyden M.A., de Boer T.P., Passier R. et al. Cardiomyocytes from human and mouse embryonic stem cells. *Methods in Molecular Medicine* 140: 249-272 (2007).

2 Takahashi K., Yamanaka S. Induction of pluripotent stem cells from mouse embryonic and adult fibroblast cultures by defined factors. *Cell* 126: 663-676 (2006).

3 Carey B.W., Markoulaki S., Hanna J., Saha K. et al. Reprogramming of murine and human somatic cells using a single polycistronic vector. *Proceedings of the National Academy of Sciences of the United States of America* 106: 157-162 (2009).

4 Warlich E., Kuehle J., Cantz T., Brugman M.H. et al. Lentiviral vector design and imaging approaches to visualize the early stages of cellular reprogramming. *Molecular Therapy* 19: 782-789 (2011).

5 Freund C., Ward-van Oostwaard D., Monshouwer-Kloots J., van den Brink S. et al. Insulin redirects differentiation from cardiogenic mesoderm and endoderm to neuroectoderm in differentiating human embryonic stem cells. *Stem Cells* 26: 724-733 (2008).

6 Freund C., Davis R.P., Gkatzis K., Ward-van Oostwaard D., Mummery C.L. The first reported generation of human induced pluripotent stem cells (iPS cells) and iPS cell-derived cardiomyocytes in the Netherlands. *Netherlands Heart Journal* 18: 51-54 (2010).

7 Davis R.P., Grandela C., Sourris K., Hatzistavrou T. et al. Generation of human embryonic stem cell reporter knock-in lines by homologous recombination. *Current Protocols in Stem Cell Biology* Chapter 5: Unit 5B 1 1 1-34 (2009).

8 Remme C.A., Verkerk A.O., Nuyens D., van Ginneken A.C. et al. Overlap syndrome of cardiac sodium channel disease in mice carrying the equivalent mutation of human SCN5A-1795insD. *Circulation* 114: 2584-2594 (2006).

9 Szuhai K., Tanke H.J. COBRA: combined binary ratio labeling of nucleic-acid probes for multi-color fluorescence in situ hybridization karyotyping. *Nature Protocols* 1: 264-275 (2006).